UNIVERSITY OF JYVÄSKYLÄ
DEPARTMENT OF CHEMISTRY
RESEARCH REPORT No. 137

VIBRATIONAL DYNAMICS OF IODINE MOLECULE AND ITS COMPLEXES IN SOLID KRYPTON

Towards coherent control of bimolecular reactions?

BY

TIINA KIVINIEMI

Academic Dissertation
for the Degree of
Doctor of Philosophy

Jyväskylä, Finland
2010

DEPARTMENT OF CHEMISTRY, UNIVERSITY OF JYVÄSKYLÄ
RESEARCH REPORT No. 137

VIBRATIONAL DYNAMICS OF IODINE MOLECULE AND ITS COMPLEXES IN SOLID KRYPTON

Towards coherent control of bimolecular reactions?

BY

TIINA KIVINIEMI

Academic Dissertation
for the degree of
Doctor of Philosophy

To be presented, by permission of the Faculty of Mathematics and Science of the University of Jyväskylä, for public examination in Auditorium FYS1, on June 24th 2010, at 12 noon

UNIVERSITY OF JYVÄSKYLÄ

Jyväskylä, Finland
ISBN 978-951-39-3914-4
ISSN 0357-346X

URN:ISBN:978-951-39-9879-0
ISBN 978-951-39-9879-0 (PDF)
ISSN 0357-346X

Jyväskylän yliopisto, 2023

Abstract

Kiviniemi, Tiina
Vibrational dynamics of iodine molecule and its complexes in solid krypton: Towards coherent control of bimolecular reactions?
Jyväskylä: University of Jyväskylä, 2010, 74 pp.
Department of Chemistry, University of Jyväskylä Research Report
ISSN 0357-346X; 137
ISBN 978-951-39-3914-4
Diss.

Iodine molecule and its 1:1 complexes with xenon atom and benzene (Bz) molecule isolated in low-temperature solid krypton environment are studied experimentally using UV-vis and FTIR absorption, resonance Raman, and femtosecond coherent anti-Stokes Raman scattering (fs-CARS) measurements. Vibrational parameters for iodine molecule on the ground electronic state, dephasing rates for the ground state vibrations, dephasing mechanisms, and structures for both of the complexes are determined.

In I_2–Xe and I_2–Bz samples, polarization interference between the different molecular species in the sample is detected in the fs-CARS signal. This interference is shown to be a useful spectroscopic tool, with which the properties of a weak signal species can be determined. The use of polarization beating as an "amplifier" is demonstrated for weak signals from both I_2–Xe complex and benzene molecule. The polarization beats are succesfully used to find out the vibrational properties of these systems.

Additionally, a general recipe for executing coherent control of a bimolecular charge-transfer reaction using a fs-CARS scheme is outlined. The experimental results obtained for the I_2–Xe and I_2–Bz complexes in this work are evaluated from the reaction control point of view. In the light of the experimental results, both of these complexes are considered promising candidates for bimolecular reaction control experiments.

Keywords

Femtosecond spectroscopy, femtosecond coherent anti-Stokes Raman scattering (fs-CARS), vibrational dynamics, coherent control, iodine molecule, iodine-benzene complex, iodine-xenon complex, matrix isolation

Author's address Tiina Kiviniemi
Department of Chemistry
Nanoscience Center
P.O. Box 35
40014 University of Jyväskylä
Finland
tiina.t.kiviniemi@jyu.fi

Supervisor Prof. Mika Pettersson
Department of Chemistry
Nanoscience Center
P.O. Box 35
40014 University of Jyväskylä
Finland

Reviewers Prof. Lauri Halonen
Laboratory of Physical Chemistry
Department of Chemistry
University of Helsinki
Finland

Prof. Matti Hotokka
Laboratory of Physical Chemistry
Åbo Akademi University
Finland

Opponent Dr. Claudine Crépin-Gilbert
Institut des Sciences Moléculaires d'Orsay - CNRS -
Université Paris-Sud
France

Preface

The work included in this thesis was carried out in the Department of Chemistry in the University of Jyväskylä during 2003–2010. These years have passed at an incredible speed, and I have been lucky to be surrounded by so many talented, enthusiastic, and supportive people. I owe to them all for helping me through this demanding, but also rewarding time.

I am deeply grateful for Professor Mika Pettersson for offering me this opportunity to work in such an interesting field, and for believing in me and my work also during the periods when I myself was in doubt. Mika has been the most supportive, enthusiastic, and visionary supervisor, and I truly owe him a lot for learning so much in the course of this work. I also wish to thank professors Henrik Kunttu and Jouko Korppi-Tommola for their interest and support, and for welcoming us as a part of the Physical Chemistry group in Jyväskylä.

Of course, I haven't done this work alone. The biggest thanks go to my dear colleagues M.Sc. Eero Hulkko, who has shared the ups and downs in the darkness of the lab with me and asked very difficult but important questions forcing me to deepen my understanding of this work, and to Dr. Toni Kiljunen, who has provided us with not only computational data but also excellent questions and explanations. I also owe a lot to Dr. Pasi Myllyperkiö, Dr. Jussi Ahokas, and M.Sc. Jukka Aumanen for the practical help in the lab. All the people from Physical Chemistry Department, past and present, along with the Organic Chemistry and Physics hangarounds, have participated in creating a pleasant working environment, of which I'm truly grateful. From the very beginning of my post here I have felt welcome and a part of this jolly group of scientists and its all thanks to you. I'm happy to call many of you not only my colleagues but also my friends now.

All work and no play would not have been an option for me, which is why I wish to acknowledge my dear friends too. Thank you for being there for me and for taking my mind off the science every now and then. Hanna and Arto, Antti and Hanna, Mikko and Terhi, Jussi and Taina, Valtteri, Jari, the underwater friends from Jyväskylän Sukeltajat and all the others, I'm lucky to have you to keep me relatively sane. The same goes for my family, that has always supported whatever endeavours I have chosen to take on - my mother Eeva, father Arto, grandmother Marja-Terttu, lovely sisters Katja and Suvi with their families, and my "family by marriage", the Ahonens and Walkers, thank you for being there for me and making my life so pleasant. Last but definitely not least, I thank my beloved husband Ville for his everyday love, support and understanding. Without you, I would not be here today.

Finally, I wish to thank the reviewers of this thesis, professors Lauri

Halonen and Matti Hotokka for their valuable work and helpful comments. The financial support from the Academy of Finland is gratefully acknowledged, and rector Aino Sallinen is thanked for the Konnevesi grant that allowed me to concentrate intensively on the finalizing of this thesis.

Jyväskylä, May 24th 2010

Tiina Kiviniemi

List of original publications

This thesis is a review based on the original publications listed below and they are herein referred to by their Roman numerals.

I **Time-resolved coherent anti-Stokes Raman-scattering measurements of I_2 in solid Kr: Vibrational dephasing on the ground electronic state at 2.6–32 K.**
T. Kiviniemi, J. Aumanen, P. Myllyperkiö, V. A. Apkarian, and M. Pettersson, *J. Chem. Phys.* **2005**, *123*, 064509.
https://doi.org/10.1063/1.1990115

II **Time-resolved coherent anti-Stokes Raman-scattering polarization beat spectroscopy of I_2–Xe complex in solid krypton.**
T. Kiviniemi, T. Kiljunen, and M. Pettersson, *J. Chem. Phys.* **2006**, *125*, 164302.
https://doi.org/10.1063/1.2358987

III **Vibrational Characterization of the 1:1 Iodine–Benzene Complex Isolated in Solid Krypton.**
T. Kiviniemi, E. Hulkko, T. Kiljunen, and M. Pettersson, *J. Phys. Chem. A* **2008**, *112*, 5025–5027.
https://doi.org/10.1021/jp801980k

IV **Iodine–Benzene Complex as a Candidate for a Real-Time Control of a Bimolecular Reaction. Spectroscopic Studies of the Properties of the 1:1 Complex Isolated in Solid Krypton.**
T. Kiviniemi, E. Hulkko, T. Kiljunen, and M. Pettersson, *J. Phys. Chem. A* **2009**, *113*, 6326–6333.
https://doi.org/10.1021/jp902012u

V **Impulsive excitation of high vibrational states in a I_2 Xe complex on the electronic ground state.**
T. Kiviniemi, E. Hulkko, and M. Pettersson, *Chem. Phys. Lett.* **2010**, *491*, 44–48.
https://doi.org/10.1016/j.cplett.2010.03.075

Author's contribution

In Paper I, the author has participated in the measurements, analyzed most of the experimental data, and written the parts II and III (Experimental details and Experimental analysis).

In Paper II, the author has had a major role in all the measurements, analyzed the experimental data, and written the parts II–IV (Theoretical background, Experimental details and Experimental results), as well as sections of part VII (Discussion) and VIII (Conclusions).

In Papers III–V, the author is the corresponding author. In these papers, she has had a major role in the fs-CARS and resonance Raman measurements, and participated in the UV-vis and IR measurements, analyzed the experimental fs-CARS and resonance Raman data, and written all parts of the papers.

Abbreviations

Bz	benzene, C_6H_6
BBO	β-barium borate
CARS	coherent anti-Stokes Raman scattering
CT	charge-transfer
FFT	fast Fourier transform
fs	femtosecond, 10^{-15} s
FTIR	Fourier transform infrared
FWM	four-wave-mixing
IR	infrared
NOPA	non-collinear optical parametric amplifier
PMT	photomultiplier tube
UV	ultraviolet
vis	visible

Contents

1 Introduction

In the very heart of chemistry lies the desire to be able to interrogate and manipulate atoms, molecules, and their reactions. The development of methods to either find out the detailed properties of molecules, or to control the outcomes of reactions, is one of the central problems in chemistry. The more traditional reaction control methods, widely used in the chemical industry, are based on the adjustment of factors such as temperature, pressure and catalysts, but also photochemistry can be used to affect the outcome of a reaction. Optical spectroscopy, which is essentially the study of interaction of electromagnetic radiation with atoms and molecules, has become a standard means of finding out the properties of chemical systems. Ever since the dawn of lasers in the 1960's, ideas and studies for using laser radiation as a means to affect the outcome of reactions have escalated rapidly. The emergence of methods for producing ultrashort laser pulses in the 1980's, enabling following and affecting molecular motions in "real time", opened up a vast new field of questions, ideas, and possibilities on the study and control of chemical reactions. This is the field where this thesis is situated; it is a small part of the ongoing quest for more and more sophisticated methods for interrogating and controlling chemical reactions in every detail.

1.1 Femtochemistry and coherent control

Femtochemistry is a field of photochemistry, where temporarily very short laser pulses, less than 100 femtoseconds (10^{-15} s) in duration, are used to study and manipulate molecules and their reactions. The duration of a femtosecond pulse is shorter than a typical vibrational period of a molecule, so that during the influence of the pulse, the nuclei in the molecule will not have moved significantly. This allows the study of real-time dynamics of chemical systems and processes via "snapshots" of nuclear motions, similarly to photography. The dynamics of a molecule or a reaction is followed by using a probe pulse that interrogates the state of the system after a well-defined evolution time, creating a signal that can be measured. By changing

the timing of the probe pulse, the evolution can be recorded step by step, creating a motion picture of the process. To obtain an accurate description of the time evolution of the system, the starting point of the process needs to be known accurately, as well as the timing of the probe pulse. Additionally, the experimental detection limitations usually demand the process to be synchronized for a large amount of molecules in order to produce a signal with a measurable strength. For these reasons, the reaction or process under study is initiated with a femtosecond pump pulse, or with a combination of several pulses. Usually, all the laser pulses used in an experiment are initially generated in the same source, after which the time difference between them can be changed by routing the probe pulse via a path with variable length. Carefully changing the path length of the probe pulse allows recording the signal as a function of the evolution time, and the changes in the signal can then be interpreted in terms of changes in the system, creating a picture of its time evolution.[1–3]

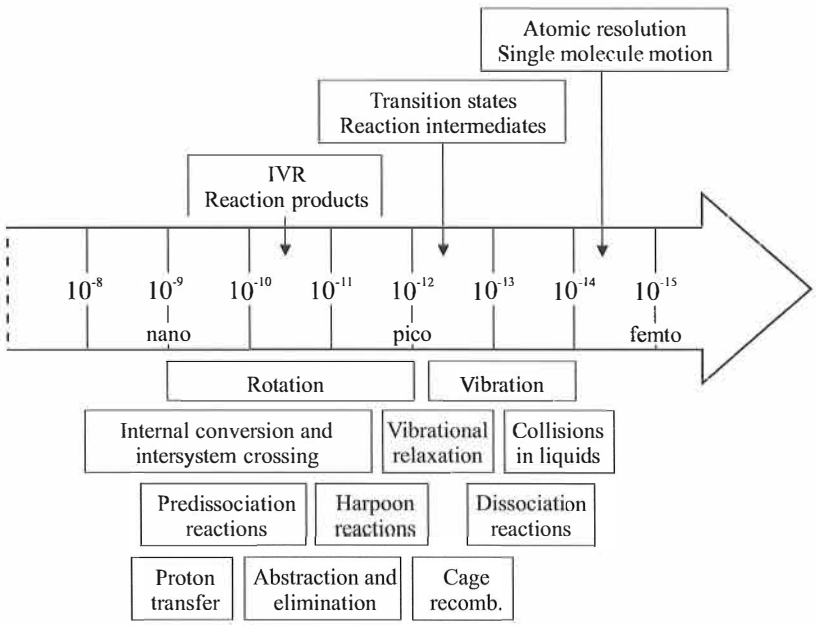

Figure 1.1: Timescales relevant for femtosecond studies and examples of different phenomena detectable in these timescales. Figure adapted from Zewail.[2]

Femtosecond spectroscopy becomes a useful tool whenever the studied phenomena are taking place at a timescale shorter than what can be studied with more conventional methods. Thus, the field of femtochemistry covers a vast area of chemical and physical processes, some of which are summarized in Figure 1.1. The studies cover molecular dynamics on different states of molecules in systems varying in size from a diatomic molecule to clusters or proteins, in different phases of matter from gas to solid, molecular beams to surfaces and interfaces, and from small droplets to nanoparticles. A very natural field of study for femtochemistry includes different aspects of fast chemical reactions such as dissociation, isomerization, intramolecular energy relaxation, electron and energy transfer, and detection and dynamics of transition states.[1–4] More applications are developed continuously, and ever shorter timescales, beyond femtosecond, can already be reached.[5]

Femtosecond spectroscopy methods, with the pump and probe pulses affecting and detecting the molecular motions in real time, also contain intriguing tools for manipulating the dynamics of the systems. Before the age of femtosecond laser sources, reaction control was attempted with longer, highly monochromatic pulses or with continuous-wave lasers in order to pump energy in a single bond to reach selective dissociation. However, this approach was not very succesful due to fast intramolecular vibrational energy redistribution in the molecular systems. With femtosecond pulses, however, the timescale for the manipulation of the molecular systems became much shorter than the vibrational energy redistribution times, opening up new possibilities in this field, as was suggested by Zewail already in 1980.[6] The coherent motion of the system from the transition state to the products could be followed in real time, which naturally led to an idea of optimizing the femtosecond laser pulse sequences in order to enhance the desired reaction pathway. Ever since, the coherent laser control of chemical reactions has been of keen interest to numerous research groups all over the world, and several reviews on the topic have been published, covering different aspects of reaction control, from fully theoretical approaches to practical experimental realization schemes.[3,4,7–15]

Several different schemes for realizing coherent reaction control have been proposed over the years. Some of the best known schemes are the Tannor-Rice-Kosloff scheme, where the evolution of the system is manipulated in time domain with short laser pulses,[16–18] and the Brumer-Shapiro scheme, which exploits interferences between different light-induced reaction pathways.[19,20] In simple model systems, both of these concepts can be considered and realized as single-parameter control schemes, where the change in only one parameter (the time delay between the pulses or the phase difference between two laser fields) induces the change in the outcome of the

reaction. In addition, the effect of time-frequency modulation of the pulse, or chirp, has been used as a control parameter in the reaction control studies.[15,21–26] With larger molecular systems, however, the schemes needed to reach a desired reaction may be very difficult to predict, which has led to the development of evolutionary algotrithms for the reaction control.[10,15,27–29]

The time-domain reaction control scheme proposed by Tannor, Rice and Kosloff is a rather intuitive model, when considering the motion of a wavepacket on a potential surface, and the interaction of the system with light. The general idea is to generate a localized wavepacket, i.e. a time-dependent superposition of selected eigenstates of the system, on a selected potential surface of the molecular system, which is then allowed to evolve. During the evolution time, the wavepacket will probe different areas of the potential surface until it reaches a proper shape and position. Then, another pulse is used to move the wavepacket on a reactive surface in a position that leads to the desired reaction.[17,18] The control parameter in the simplest case of this scheme is only the time delay between the two laser pulses, and the control process resembles the pump-probe or pump-dump scheme routinely used in spectroscopic femtosecond applications. However, the evolving wavepacket can just as well be created on the ground electronic surface by adding another pulse to the excitation part of the control process, so that the wavepacket is generated with a pump-dump scheme, and a third pulse is used for the final control step.[17] In addition, the shape of each pulse in the control process can be optimized in frequency and intensity to achieve more detailed control on the wavepacket properties.[21] The use of Tannor-Rice-Kosloff scheme has been demonstrated experimentally for several different unimolecular reactions of small molecules, such as ionization and fragmenta tion reactions.[8,11]

Any coherent control scheme can in principle be realized with predesigned control parameters, assuming that the system under control is known in adequate detail. However, as the systems grow in size and complexity, it is clear that an accurate calculation and predesign of the needed pulse properties becomes more and more difficult, if not impossible. Moreover, the exact experimental generation of the desired pulse properties may suffer from errors, which, however small, can have a large effect on the outcome of the reaction. To overcome these problems, Judson and Rabitz suggested in 1992, that rather than trying to solve the problem beforehand, an iterative setup could be used to "teach the lasers to control molecules".[27] In short, this kind of system consists of a pulse shaper and an evolutionary algorithm program, which is used to optimize the yield of the desired product based on the measured signal. Using the feedback from the signal, the different field characteristics are evaluated and modified by the program, until the best

possible yield is obtained.[10,11,27] After the first realizations of this scheme by Bardeen *et al.*,[30] and Assion *et al.*,[29] several experiments using this adaptive control scheme have been realized, including control of atomic ionization, selective bond breakage, and branching ratio in a dissociation reaction of a polyatomic molecule.[10,11]

The adaptive control scheme is attractive from the experimental point of view in the sense that the experimentalist doesn't have to personally participate in the adjustment of each field tested for control. Accordingly, the technique is sometimes referred to as the "black box" technique, pointing to the fact that gaining optimum yield for a reaction may not be satisfactory from the scientific point of view, which aims for understanding the processes. With the evolutionary algorithm, impressive results in optimizing a reaction yield can in practice be obtained without any understanding of the mechanisms that lead to them. Also, with enormous amount of different pulse possibilities, it might be difficult to determine if the field obtained through the algorithm is truly the converged optimum solution or not.[10,11,15] However, the understanding of the process can be gained afterwards; the analysis of the optimum field obtained can be used to extract information on the system under control, and on the reaction process. Depending on the process, the explanation can nevertheless be expected to demand approximately as much theoretical effort as figuring out beforehand the optimum fields for a well-known system.

Regardless of the reaction control scheme, the experimental realizations of the coherent control have so far involved mainly unimolecular reactions.[11] From the amount of data gained over the years, it is obvious, that unimolecular reactions are at least to some extent controllable with laser pulses. However, controlling bimolecular reactions still seems a rather demanding area of study, and no clear evidence on a successful coherent control experiment of a bimolecular reaction has been published yet despite of a few attempts.[11,31,32] In practice, femtosecond chemistry techniques are already at the level where the imagination of the researchers sets the limit to the different experimental approaches. The challenges lie more in the nature itself; how to affect a bimolecular system as a whole to reach a desired outcome - and how to prove that the control really took place? Because of this, selecting a good, simple model system is of crucial importance in the attempts to achieve coherent control of a bimolecular reaction.

1.2 Spectroscopy of the iodine molecule and its complexes

The iodine molecule, I_2, is a homonuclear diatomic molecule with well known properties. Experimentally, it is easy and safe to handle, cheap to purchase, and with an electronic absorption in the visible part of the spectrum, it is easy to study with conventional lasers and light sources. Moreover, it has a rather narrow vibrational energy level spacing on its ground electronic state, making creation of vibrational wavepackets possible. The spectroscopic properties of the iodine molecule have been under a thorough study over the decades both experimentally and theoretically, and the amount of data on the iodine molecule is immense. Thus, the potential curves of its ground and excited states can be claimed to be well known (see, for example, Herzberg[33] and Jong *et al.*,[34] and references therein). These features make the iodine molecule an attractive model system for all kinds of studies from undergraduate laboratory demonstrations to femtosecond spectroscopy experiments on dynamics and control.

The iodine molecule was the first bound system for which vibrational and rotational motions were resolved in real time using femtosecond pulses.[35–37] The pump-probe experiments by the Zewail group revealed the vibrational motion on the electronic B state of the gas-phase molecule, and explained it as the motion of the coherent wavepacket on the electronic potential surface. After that, the study of femtosecond dynamics has expanded to all kinds of systems, but iodine molecule has remained an interesting object of study. For example, the vibrational dynamics and predissociation process on the B state of iodine have been thoroughly studied,[38–44] together with the cage effect in dissociation processes in rare-gas clusters and matrices.[45–48]

The vibrational dynamics of iodine molecule on the ground electronic state, that is of special interest in this thesis, are difficult to probe with steady-state spectroscopy like spontaneous resonance Raman scattering, as the instrumental resolution may be insufficient for detecting the real linewidths for the long-lived vibrations at least at lower temperatures.[49–51,I,III–V] With femtosecond techniques, however, the dynamics on the ground electronic state has been studied extensively using fs-CARS and degenerate four-wave-mixing (DFWM) techniques in both gas phase[25,52–67] and isolated in solid matrices.[38,68–72,I] In gas phase, the signal is complicated due to the simultaneous rotational coherence, but in solid phase, the rotation is restricted so that only vibrational dynamics on the ground electronic state is detected. The experiments in solid matrices also give interesting information on the dephasing mechanism of the vibrations and thus, on the coupling of the sys-

tem to the environment. The low temperatures used in matrix experiments allow for long vibrational dephasing times, so that the coherence lasts for hundreds of vibrational periods at the lowest vibrational states.[68–71,I]

Several coherent control experiments have also exploited the I_2 molecule. The properties of the wavepacket on the B state have been controlled and modified using phase-locked pumps in both gas phase and in solution,[73–77] with a chirped pump in both gas phase[25,26,28,78–80] and in solid rare-gas matrices,[28,81] and with a phase- and amplitude modulated pump in the gas phase.[82] The properties of the ground electronic state vibrational wavepackets in the iodine molecule have also been manipulated using different four-wave-mixing (FWM) techniques: degenerate four-wave-mixing (DFWM) for gas phase molecules[52–58,83–86] and coherent anti-Stokes Raman scattering (CARS) in gas phase[53,54,59–61,63,64,87] and in solid matrices including rare gases and ice.[38,68–71,I] All these experiments have involved manipulation of the intramolecular properties of the wavepacket rather than real reactions, but also the branching ratio of photodissociation of iodine to $I(^2P_{3/2}) + I(^2P_{3/2})$ or to $I(^2P_{3/2}) + I(^2P_{1/2})$ has been controlled by a polarized pump pulse combined with laser alignment of the molecules.[88] A coherent superposition of rovibrational states of the gas-phase iodine molecule has also been proposed to be used for manipulating and processing quantum information.[89–92]

This large amount of femtosecond and coherent control data already produced of the iodine molecule in different environments makes it a perfect model system for additional, more complex experiments. A natural step forward to more complicated systems is to study a weak complex of the iodine molecule. The weak complexation is not expected to radically change the properties of the molecule, so the use of similar schemes for manipulating and interrogating the system is possible. Via the manipulation of the iodine molecule in the complex, the whole system can be affected, opening up new research possibilities. In this thesis, two different 1:1 iodine complexes were studied, the weak complex with a xenon atom, and the slightly stronger iodine-benzene complex.

The iodine-xenon system has been studied earlier mainly as a model system for laser-assisted harpooning reactions amongst other halogen–rare-gas pairs.[93–96] In these reactions, the halogen molecule X_2 (X = F, Cl, Br, I) is excited to an ion-pair state with the presence of rare-gas atoms Rg, so that the charge-transfer between the halogen and the rare-gas atom leads to the formation of Rg^+X^- and an X atom. These reactions were among the earliest examples of gas-phase reactions induced by radiation resonant with intermolecular states, and the mechanism is of importance for a variety of reactions also in media other than the gas phase.[97]

An interesting study of the harpooning reaction between I_2 and Xe is

the experiment by Potter *et al.*,[31] which can probably be considered as the first published attempt of femtosecond control of a bimolecular reaction. In this gas-phase experiment, the iodine molecule was first excited on the B state with a femtosecond pulse creating an oscillating wavepacket. Then, a second femtosecond pulse was used at a specific moment to excite the wavepacket further to the ion-pair state, followed by a reaction with a xenon atom. The product yield was found to be oscillating as a function of the time delay between pump and control pulses, similarly to the wavepacket motion on the B state. The interpretation by Potter *et al.* was such that the control pulse excited the I_2 Xe collision complex, and by timing it to fit the I–I bond length optimal for the reaction, they could control the outcome of the reaction. Unfortunately, as was pointed out later,[32] the experiment cannot distinguish between two mechanisms; the one, where the collision complex is excited by the control pulse:

$$\begin{aligned} \mathrm{I_2}(X) + h\nu_{pump} &\rightarrow \mathrm{I_2}(B) \\ \mathrm{I_2}(B)\cdots\mathrm{Xe} + h\nu_{control} &\rightarrow \mathrm{Xe^+I_2^-} \\ &\rightarrow \mathrm{Xe^+I^-} + \mathrm{I}\ , \end{aligned} \tag{1.1}$$

and the other, where the iodine molecule alone is excited to the ion-pair state prior to a collision with the xenon atom:

$$\begin{aligned} \mathrm{I_2}(X) + h\nu_{pump} &\rightarrow \mathrm{I_2}(B) \\ \mathrm{I_2}(B) + h\nu_{control} &\rightarrow \mathrm{I^+I^-} \\ \mathrm{I^+I^-} + \mathrm{Xe} &\rightarrow \mathrm{Xe^+I^-} + \mathrm{I}\ . \end{aligned} \tag{1.2}$$

The crucial difference between these two mechanisms is that (1.1) can be regarded as coherent control of a bimolecular reaction, whereas in (1.2) the control pulse is affecting only the excitation of the iodine molecule on the ion-pair state, and the reaction can then proceed on the collisional time scale, long after the termination of the control pulse. As was argued by Apkarian,[32] the second mechanism, (1.2), can be estimated to completely overwhelm the signal in the experimental conditions of Potter *et al.* Thus, the execution of coherent control of this reaction lacks evidence unless the mechanism in (1.1) could be singled out. This kind of experiment has not yet been performed, but the problem might be overcome by either directly probing the $Xe^+I_2^-$ species, or by changing the experimental conditions so that the complex can be prepared and maintained in the entrance channel complex conformation, like in the matrix isolation technique. For example, the harpoon reaction between Xe and Cl_2 was followed by Zadoyan and Apkarian in liquid Xe by interrupting the reaction of Xe^+Cl^- with Xe by

a femtosecond dump pulse, changing the direction of the reaction.[98] Thus, considering these examples, halogen-rare-gas complexes such as iodine-xenon can be considered interesting and promising systems for additional coherent control experiments.

The other iodine complex under study in this thesis is the iodine-benzene complex. The study of the I_2–Bz complex can be considered to have begun already in the 1940's, when Benesi and Hildebrand found its UV charge-transfer (CT) absorption at ~ 280 nm in iodine-benzene solution.[99,100] This common prototype of a complex with a low-lying charge-transfer state has ever since been a subject of numerous studies trying to elucidate the structure, properties and reactions of the system. Considering the amount of work done on this complex, it is rather surprising that it took almost 60 years to find an agreement between computational and experimental results on its ground electronic state structure (see Fig. 3.5 in Section 3.3).[101–104,III] Also, experimental spectroscopic information of the actual 1:1 complex[105,106,III,IV] is not as abundant as one might expect, due to the fact that most of the measurements on the complex are done with liquid samples, where usually no distinct features of a well-defined 1:1 complex are found.[107 112]

One of the most interesting properties of the I_2–Bz complex is, however, its low-lying charge-transfer state and the processes that can be easily accessed through UV excitation. The availability of femtosecond techniques in 1990's started a new era in the study of this complex, as the charge-transfer reaction and its dynamics could now be studied in "real time".[101,102,113–116] The dynamics of the charge-transfer reaction have been studied in both liquid phase[101] and in molecular beams.[102,113–116] In the experiments by Cheng *et al.*, two main dissociation channels after the UV excitation have been found: an ionic, and a neutral channel.[113] The ionic dissociation is found to follow the ionic potential of the CT state, and to proceed via formation of the charge-transfer complex between iodine and benzene molecules with a simultaneous elongation of the I I bond to produce Bz^+I^- and I. The neutral channel, on the other hand, is due to the coupling of the transition state to a neutral, locally excited repulsive states of iodine, producing BzI and I. The neutral channel was found to be faster and resulting in a greater yield than the ionic channel.[113] Additionally, DeBoer *et al.* found a molecular channel producing molecular I_2 and Bz fragments.[115]

The several possible reaction channels implicate the complexity of the charge-transfer state potentials, but also offer a possibility to study experimentally the yields of the different reaction channels. The femtosecond technique allows using the short pulses for switching between different potential surfaces at a timescale shorter than the nuclear motion. Thus, cleverly designed pulse sequences could be used to create and guide a wavepacket to a

desired reaction channel, which might not even be accessible via a Franck-Condon excitation from the ground state of the molecule. The iodine-benzene complex might be a good candidate for this kind of studies, as the low-lying charge-transfer state can be accessed with rather standard UV wavelengths, making the experimental effort easier.

1.3 Motivation and aims of this study

The aim of the work included in this thesis is to study and control vibrational wavepackets on the ground electronic state of the iodine molecule and its complexes with the xenon atom or the benzene molecule, in order to reach the knowledge needed for the coherent control experiments. The fs-CARS method used in the experiments can be used as a pulse sequence in a Tannor-Rice-Kosloff type of reaction control with small modifications, and is thus a good means for studying properties that are interesting from the control point of view. The iodine molecule was selected as the subject of this study due to its well-known spectroscopic properties and potential energy curves. The optical properties of the iodine molecule make the experiments possible with visible laser pulses, and its vibrational time scale is sufficiently long to be probed with easily achievable pulse lengths, making it an ideal model system, as can be seen from the vast amount of data already available on its femtosecond chemistry. To gain information on bimolecular systems, I_2–Xe and I_2–Bz complexes were chosen. The I_2–Xe complex has already been studied from the coherent control point of view,[31] and is easy to prepare in a rare-gas matrix. The charge-transfer reactions of the I_2–Bz complex, on the other hand, are well-studied,[101,102,113–115] and it is also easily prepared in liquid or gas phases, enabling the extension of the results closer to "real-life" applications. All these model systems were isolated in a solid, low temperature krypton environment to enable the preparation of a well-defined 1:1 complex that can be maintained in the desired conformation, and to simplify the interpretation of the results.

In this study, ultrafast laser pulses are used to excite, interrogate, and manipulate the vibrations of the iodine molecule in its monomeric and complexed form. The interrogation and manipulation of vibrational wavepackets allows obtaining accurate data on the system studied. After gathering enough knowledge of the system's properties, the wavepackets can be designed for and used as a starting point in controlling the reaction of the system. However, to be able to execute and understand such a control experiment, detailed knowledge is required on several properties of the system. The main goal of this work was to find out detailed information on the three systems studied,

and to evaluate the experimental findings from the reaction control point of view. In the course of this work, a new kind of method for obtaining data on the complex systems, using polarization interference, was introduced and used. Although the control scheme evaluated here is not yet experimentally realized, the results obtained in this work constitute a step forward in implementing reaction control on a bimolecular system using a fs-CARS-like pulse sequence.

2 Methods

In this chapter, the basics of the experimental methods used in this study are shortly described. As the traditional methods, such as infrared absorption and spontaneous resonance Raman spectroscopy, are widely used and can be expected to be of common knowledge among chemists, their principles are not presented here. Instead, this chapter focuses on describing the methods that are not in everyday use in chemistry but are of an important role in the work presented here, namely, the matrix isolation technique that is used for sample preparation; and the femtosecond coherent anti-Stokes Raman scattering (fs-CARS) technique, which is used to manipulate and interrogate in real time the vibrations of the iodine molecule in different sample systems. The first two sections present the basics of matrix isolation and fs-CARS techniques, and the last section is intended to give a brief overview on the properties of the practical experimental setups used in this work.

2.1 Matrix isolation

Matrix isolation technique was originally developed for the study of unstable and reactive molecular species such as free radicals.[117,118] After that, the field has expanded to cover also the study of stable molecules and their interactions, and chemistry and physics in solid state.[119,120]

The general idea in matrix isolation is to isolate the system under study (guest) in a solid, usually unreactive, medium (host). The matrix medium is selected so that the interactions between the guest and host are preferably as weak as possible, to avoid large changes in the properties of the system under study. A large host-to-guest ratio, ranging typically from 100 to 10000, is usually preferred, in order to isolate the guest into a cage of host molecules only, to avoid unwanted clustering or reactions of the guest. Most commonly used hosts are rare gases from neon to xenon, and nitrogen, due to their low reactivity and weakly interacting nature. Also, the low temperature (4–70 K) needed to make solid matrices out of these gases helps to avoid diffusion of the guest molecules in the sample, preventing bimolecular reactions

from taking place. Both rare gas and nitrogen matrices are transparent from mid-infrared through visible to UV wavelengths, and are thus a good choice for a matrix material as the samples are generally studied with optical spectroscopy, although magnetic spectroscopy has also been used.[119,120]

The weak interactions between the host and guest molecules simplify the study of the system, but there are a few effects typical to matrix isolation experiments that are to be taken into account.[119] For example, the interaction of the host molecules with the guest induces a detectable change in the vibrational frequencies of the molecule when compared to the gas phase values, which is called a matrix shift. The guest molecule can also adopt different trapping sites in the matrix, depending on its shape and size. A small atom can fit into an interstitial site, located in an octahedral or tetrahedral space inside the lattice of the host atoms. A larger molecule or a molecular complex will rather occupy a substitutional site, where the guest replaces one or more of the host atoms or molecules in the lattice. Also, defect trapping sites are possible, as the matrices are rarely perfect crystals. As each of these sites produces a different kind of environment for the guest, the properties of the guest molecule are slightly modified depending on the site occupied, which can be observed, for example, as a shift in the vibrational frequencies of the molecule, or so called site-effect.

The geometry of the trapping site usually restricts rotation of the guest molecules, except for the smallest molecules such as water, hydrogen halides, and ammonia, and even for these the low temperature of the sample allows for only the lowest rotational levels to be populated.[119] Due to the low temperature, vibrational population distribution is also narrow, and at rare gas matrix temperatures the molecules are on their lowest vibrational states. In studying weak molecular complexes, the matrix isolation technique is useful, as the trapping of the complex in a solid environment fixes the system in a well-defined conformation with no interactions with other complexes, simplifying the system when compared to gas or liquid phases, where the interaction between the molecules changes dynamically due to diffusion of the species, and the study of a well-defined 1:1 complex is in practice more difficult.

There are several advantages in matrix isolation technique when considering the work presented in this thesis. Isolating the iodine molecule or its complex in a low temperature solid krypton environment suppresses the rotation of the molecule, and renders it on the lowest vibrational state, $v = 0$, of the ground electronic state, simplifying the system. The low temperature of the experiment also allows for long dephasing times of the ground electronic state vibrations, which is advantageous from the reaction control point of view, as the wavepacket has a longer time to evolve after its generation.

In addition, the interactions between the molecule and its environment are weak, and the studied molecules or complexes are isolated from each other due to the low concentration in the matrices, simplifying the explanation and simulation of the experimental results. The unwanted diffusion of the species is also suppressed. With deposition parameters, it is possible to control the amount of complexes in the sample, and when done with care, samples with only monomeric molecules or 1:1 complexes with well-defined structures and trapping sites can be obtained together with high optical density and a good optical quality. Thus, the matrix isolation technique offers a good means for creating a simplified model system for studies of manipulating, interrogating, and controlling molecules or molecular complexes in real time.

2.2 Femtosecond CARS technique

Femtosecond coherent anti-Stokes Raman scattering (fs-CARS) technique is a time-dependent, coherent, nonlinear spectroscopy method, which uses short optical laser pulses to investigate the properties of the sample. The temporal length of the laser pulses, typically < 100 fs, is shorter than the typical vibrational period of molecules, which makes the study of the "real-time" dynamics of the molecular motions possible.

The fs-CARS method is a four-wave-mixing (FWM) technique, in which three ultrashort laser pulses are used to generate a third-order polarization, which then emits a photon that is measured. The properties of the emitted photon depend on the interaction between the three laser pulses and the sample, and it has a wavelength and direction determined by the incoming laser pulses, according to the energy and momentum conservation principles.[16,121] In Figure 2.1, a schematic presentation of the CARS process is shown. The first pulse, so called pump pulse with wavevector $\mathbf{k}_{pump}$ and energy ω_{pump}, excites the molecule from the state i on the ground electronic state g to the state n on the excited electronic state e. This excitation prepares a time-dependent coherent superposition of several vibrational eigenstates, i.e. a wavepacket, on the excited state. The wavepacket then evolves on the excited state for a time t_{12}, until a second, dump pulse with $\mathbf{k}_{dump}$ and ω_{dump}, moves the system to the state j on the ground electronic state. As $\omega_{dump} < \omega_{pump}$, the wavepacket is generated on vibrational levels higher than the starting point. After evolving on the ground electronic state for a time t_{23}, the third pulse, or probe, moves the system back to the excited electronic state from which the CARS photon is emitted. The CARS photon will have an energy of $\omega_{CARS} = \omega_{pump} - \omega_{dump} + \omega_{probe}$, and direction $\mathbf{k}_{CARS} = \mathbf{k}_{pump} - \mathbf{k}_{dump} + \mathbf{k}_{probe}$. The direction in which the CARS signal is emitted is thus dependent on the

pulse geometry used in the experiment, as shown in Figures 2.1 and 2.2. The intensity of the CARS signal will depend on the times t_{12} and t_{23}, according to the processes the system undergoes while left to evolve between the pulses.

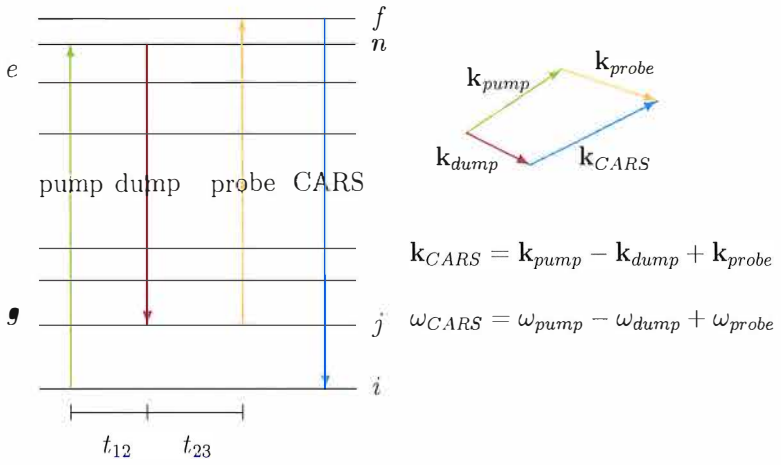

Figure 2.1: Schematic presentation of the fs-CARS process. The energy ω and direction $\mathbf{k}$ of the CARS emission is determined by the combination of the pump, dump, and probe pulse properties. In the experiments, either time t_{12} or t_{23} is scanned, so that the signal shows the dynamics of the excited or ground electronic state, respectively. Due to the large bandwidth of the exciting laser pulses, the states j, n, and f should be considered as manifolds of several vibrational states.

According to the uncertainty relation, $\Delta t \Delta E \leq \hbar$, a very short laser pulse will have a wide energy distribution. When considering femtosecond pulses, the energy distribution of the pulses is wide enough to excite several vibrational states of the molecule coherently, creating a superposition of several vibrational eigenstates, or a time-dependent wavepacket. Thus, in fs-CARS process, each energy level in Figure 2.1 should be considered as a manifold of vibrational states, which are all excited within the large bandwidth of the short laser pulse, rather than a single eigenstate of the molecule. In addition, the fs-CARS process does not have to be electronically resonant, but the e state can also be a virtual state similarly to the spontaneous Raman process.[16] However, electronic resonance notably enchances the fs-CARS signal, and is thus often exploited in experiments.[122]

The theoretical description of the fs-CARS signal has been presented in several studies.[16,87,121,123] In practice, it involves the calculation of the

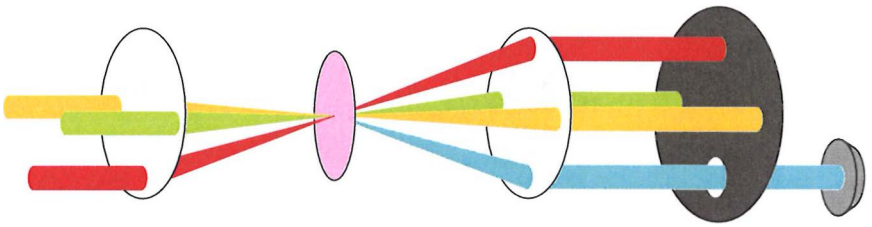

Figure 2.2: The "boxcar" pulse geometry common in fs-CARS experiments. The direction of the pump, dump, and probe pulses determines the direction of the CARS signal generated in the sample. The boxcar geometry allows simple spatial filtering of the signal from the excitation beams, and is often used in experimental setups.

time-dependent third order polarization created in the sample by the three laser pulses. In the experiment, all light emitted to the $\mathbf{k}_{CARS}$ direction is measured as a function of either t_{12} or t_{23}. Usually, only one of the delays is changed during measurement; the signal as a function of t_{12} probes the dynamics on the excited electronic state, whereas the signal as a function of t_{23} reveals the dynamics on the ground electronic state.[16,59,87,123,124] However, the other time delay can be used for optimizing the signal, although not scanned during the measurement.[59,60]

If no restrictions are set for the timing and energies of the laser pulses, the fs-CARS signal can consist of several different processes or spectroscopic pathways.[52,87] In practice, however, many of these pathways can be eliminated by controlling the temporal order of the three laser pulses, and by selecting the pulse properties in a particular way. By arranging the timing of the pulses so that they arrive at the sample in the pump–dump–probe order, and by selecting the dump pulse energy so that it is not resonant with either $i \rightarrow n$ or $i \rightarrow f$ transitions, it is possible to eliminate all the other spectroscopic pathways and to obtain a signal consisting only of the process presented in Figure 2.1.[87] Then, the third order polarization can be calculated as:[16,87]

$$P^{(3)}_{\mathbf{k}_{\mathrm{AS}}}(t) = \langle \Psi^{(0)}(t)|\hat{\mu}|\Psi^{(3)}_{\mathbf{k}_{pump}-\mathbf{k}_{dump}+\mathbf{k}_{probe}}(t)\rangle + \text{c.c.} \tag{2.1}$$

First, we treat the case where there is only one type of species contributing to the time-dependent CARS signal in the sample. In this case, for a fs-CARS process of $|gi\rangle \rightarrow |en\rangle \rightarrow |gj\rangle \rightarrow |ef\rangle$ as in Figure 2.1, the

polarization can be presented as[16,87,121,123]

$$\begin{aligned} P^{CARS}(T) &= \frac{-i}{\hbar^3}\sum_{fjn}\mu_{if}\int_{-\infty}^{T}dT_3\int_{-\infty}^{T_3+t_{32}}dT_2\int_{-\infty}^{T_2+t_{21}}dT_1 \\ &\times \mathrm{e}^{-i\omega_{fi}T}(\mu_{fj}E_3(T_3)\mathrm{e}^{-i(\omega_3-\omega_{fj})T_3}) \\ &\times \mathrm{e}^{-i\omega_{ji}t_{32}}(\mu_{jn}E_2^*(T_2)\mathrm{e}^{i(\omega_2-\omega_{nj})T_2}) \\ &\times \mathrm{e}^{-i\omega_{ni}t_{21}}(\mu_{ni}E_1(T_1)\mathrm{e}^{-i(\omega_1-\omega_{ni})T_1}) + \mathrm{c.c.}\,, \end{aligned} \tag{2.2}$$

where μ_{xy} are the transition dipoles between the states x and y, $\omega_{xy} = \omega_x - \omega_y$, and the $\mathrm{e}^{-i\omega_{xy}t}$ terms describe the time evolution of the wavepacket on the state x for a time t after interaction with a laser pulse, that can be presented as $E_\chi(T_\chi)\mathrm{e}^{-i(\omega_\chi-\omega_{xy})T_\chi}$, where ω_χ is the carrier frequency and $E_\chi(T_\chi)$ is the laser pulse envelope.[16,87] The convolution of partial Fourier transforms of the pulse envelopes at the difference between the carrier frequency and the appropriate transition frequency along the path can be defined as

$$\begin{aligned} G_{fjni}(T) &= \int_{\infty}^{T}dT_3\mu_{fj}E_3(T_3)\mathrm{c}^{-i(\omega_3-\omega_{fi})T_3} \\ &\times \int_{-\infty}^{T_3+t_{32}}dT_2\mu_{jn}E_2^*(T_2)\mathrm{e}^{i(\omega_2-\omega_{nj})T_2} \\ &\times \int_{-\infty}^{T_2+t_{21}}dT_1\mu_{ni}E_1(T_1)\mathrm{e}^{-i(\omega_1-\omega_{ni})T_1}\,, \end{aligned} \tag{2.3}$$

which is responsible for the different amplitudes of different vibrational eigenstates in the wavepacket. By defining the polarization amplitude as

$$a_f(T) = \mu_{if}\sum_{jn}\mathrm{e}^{-i\omega_{ji}t_{32}}\mathrm{e}^{-i\omega_{ni}t_{21}}G_{fjni}(T), \tag{2.4}$$

the time-dependent fs-CARS polarization can be presented as:

$$P^{CARS}(T) = \frac{i}{\hbar^3}\sum_{f}a_f(T)\mathrm{e}^{-i\omega_{fi}T} + \mathrm{c.c.} \tag{2.5}$$

The fs-CARS signal emitted from the sample is measured with a square-law detector, so the signal is proportional to the square of the polarization integrated over time:

$$\begin{aligned} S &= \int_{-\infty}^{\infty}dT|P^{CARS}(T)|^2 \\ &= \frac{2}{\hbar^6}\sum_{ff'}\int_{-\infty}^{\infty}dTa_f(T)a_{f'}^*(T)\mathrm{e}^{-i(\omega_f-\omega_{f'})T}\,, \end{aligned} \tag{2.6}$$

where the rapidly oscillating terms (with $\omega_f + \omega_{f'}$) have been neglected according to the rotating wave approximation.[16,87]

When the probe delay t_{32} is scanned, the signal will oscillate due to the product of the polarization amplitudes a_f and $a_{f'}$:

$$a_f(T)a^*_{f'}(T) = \mu_{if}\mu_{if'} \sum_{jj',nn'} \mathrm{e}^{-i(\omega_{ji}-\omega_{j'i})t_{32}} \mathrm{e}^{-i(\omega_{ni}-\omega_{n'i})t_{21}} \times G_{fjni}(T)G^*_{f'j'n'i}(T). \quad (2.7)$$

This interference, showing oscillations at frequencies $(\omega_{ji} - \omega_{j'i})$, arises from the coherent evolution of the quantum wave function, and may thus originate within a single molecule. The oscillations, called quantum beats, reveal the vibrational structure of the system as difference frequencies of the vibrational states j involved in the wavepacket generated by the pump-dump process. A similar equation can be obtained, if the time delay between pump and dump pulses, t_{12}, is scanned instead of the probe delay, but then the signal will oscillate at the $(\omega_{ni} - \omega_{n'i})$ frequencies, telling us about the excited state properties rather than those of the ground state. If additionally the transition moment μ_{if} is approximated to be the same for all the transitions involved, $\mu_{if} = \mu$, the signal can be estimated as a sum of oscillating terms:[68,II]

$$S \propto \mu^2 \sum_{v,v'} g_v g_{v'} \cos[\omega_{v,v'} t_{32}] , \quad (2.8)$$

where g_v terms are the amplitudes of a given eigenstate v in the wavepacket generated by the laser pulse sequence, and the symbol v is substituted for j to emphasize the connection to the vibrational eigenstates of the system.

Equation 2.8 gives an oscillating signal with no decay over time, which is different from the observed fs-CARS signals. The decay in the observed signal is due to dephasing, or the loss of the phase correlation between the amplitudes of the different states, and can be seen in the frequency domain spectra as the linewidth of the spectral transitions.[121,122,125–128] The dephasing process is a result of the interactions between the molecule and its environment, and for a homogeneous sample it can be divided into two contributions; pure dephasing, due to elastic collisions between the molecule and its environment, and population- or energy relaxation, where the excited state population of the molecule is lost due to inelastic collisions with the environment.[127 129] Experimentally, the direct identification between the two mechanisms is impossible, but usually in condensed media the pure dephasing, which has a stronger temperature dependence, dominates, until it is suppressed in the limit of $T \to 0$.[68,125,126,I] In addition, the inhomogeneity of the sample may add to the linewidths, as the microscopic environment

of the molecules in the sample varies, leading to a distribution of transition energies. Thus, temperature dependent measurements with a proper control on the sample properties are needed in order to experimentally assign these different contributions.[68–70,125,I] In the end, the analysis of the temperature dependence of the dephasing rates will give information on the interactions between the molecule and its environment.[69–71,125,I]

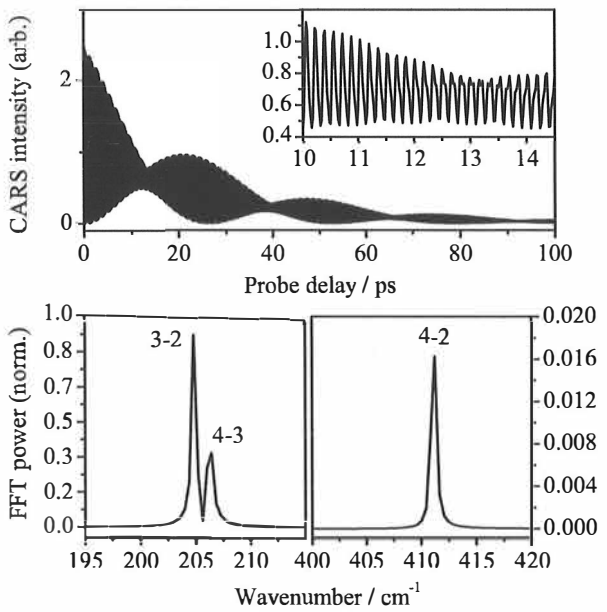

Figure 2.3: Simulation of a fs-CARS signal of a $v = 2$–4 wavepacket of iodine and its Fourier transform. Upper panel: time domain fs-CARS signal. The inset shows the fast oscillation at the $\omega_{v,v'}$ frequencies, and the slowly oscillating envelope is due to the anharmonicity of the iodine molecule. Lower panels: FFT of the time domain signal, i.e. the frequency domain signal. The oscillation frequencies are easy to determine from the frequency domain spectrum, and are labelled according to the vibrational levels associated with the vibration, for example 3–2 corresponds to the frequency $\omega_{3,2'} = \omega_3 - \omega_2$. The bandwidths in the frequency domain are determined by the dephasing rates associated with the corresponding vibrations.

To account for the dephasing, an exponential term $e^{-(\gamma_v+\gamma_{v'})t_{32}}$ can be added to Equation (2.8), with γ_v being a dephasing rate specific to a vibra-

tional eigenstate:[71,121]

$$S \propto \mu^2 \sum_{v,v'} g_v g_{v'} \cos[\omega_{v,v'} t_{32}] \mathrm{e}^{-(\gamma_v+\gamma_{v'})t_{32}} \tag{2.9}$$

As a result, a decaying signal oscillating as a function of the probe delay, with frequencies $\omega_{v,v'}$, is obtained. The $\omega_{v,v'}$ terms will give directly the difference frequencies of the vibrational energy levels in question. In addition, the signal will decay according to the dephasing rates γ_v. With several different eigenstates involved in the wavepacket, there are several different oscillation frequencies in the signal, allowing vibrational analysis of the system, and solving of the dephasing rates, thus yielding information on the system. In Figure 2.3, a simulation of the fs-CARS signal for iodine molecule in solid krypton is shown to illustrate the features of the signal, together with its Fourier transform. In the signal, fast oscillation at the $\omega_{v,v'}$ frequencies is observed with a slow decay of the signal due to dephasing. The anharmonicity of the iodine molecule vibrations creates the slowly oscillating envelope in the signal. The frequency domain, or the Fourier transform of the time domain signal, reveals the oscillation frequencies as the band positions, and the dephasing rates can be determined from the bandwidths. The Fourier transform of Equation (2.9) gives a Lorentzian lineshape for the bands with a bandwidth of $2(\gamma_v + \gamma_{v'})$.

2.2.1 Polarization beats

As was shown previously, in the case of only one type of species contributing to the fs-CARS spectrum of the sample, the signal consists of quantum beats according to Equation (2.9). However, if there are additional species contributing to the same signal, an intermolecular effect called polarization beating is observed in the fs-CARS spectrum, due to the interference of the radiation from different species. One of the main results in this work was to use these beats to obtain spectroscopic information on the different low concentration species in the systems studied. In this section, the formation of polarization beats in the signal, and their use as a spectroscopic tool, is briefly discussed.

To observe polarization beats in the fs-CARS signal, at least two different species, with different vibrational frequencies, contributing to the third order polarization (Eq. 2.1) have to be present in the sample. In practice, this means that both of the species need to have vibrational states at the pump-dump window of the pulse series, so that the preparation of a coherence on the ground electronic state is possible. In addition, to observe polarization beats, the final CARS polarization spectra of the different species have to

overlap, i.e. the polarization has to be short-lived, as was shown by Faeder *et al.*[87] If these two conditions are fulfilled, polarization beating can be observed in any kind of system. In this work, polarization beats have been found between the uncomplexed iodine molecule and the I_2–Xe complex,[II,V] and uncomplexed iodine and benzene molecules,[IV] in solid krypton matrices. Polarization beats in iodine samples have also been studied, for example, by Knopp *et al.* in the experiments with the iodine molecule in the gas phase, where the polarization beats were a result of three different initial states of the iodine molecule,[59] and by Bihary *et al.*, who studied polarization beats arising from lattice vacancies around iodine molecules trapped in solid argon matrix.[72] In addition, polarization beating has been detected between different molecules in both gas and liquid phase,[130–132] and in semiconductors.[133,134]

According to Equation (2.5), when adding the contribution of the other species to the signal, the third order CARS polarization can be expressed as a sum of the polarizations of the different species x:[87]

$$P^{CARS}(T) = \frac{-i}{\hbar^3} \sum_{ifx} p_x a_{fi}(T) \mathrm{e}^{-i\omega_{fi}T} + \text{c.c.}\,, \tag{2.10}$$

where

$$a_{fi}(T) = \mu_{if} \sum_{jn} \mathrm{e}^{-i\omega_{ji}t_{32}} \mathrm{e}^{-i\omega_{ni}t_{21}} G_{fjni}(T), \tag{2.11}$$

and p_x is the weight factor for the species x, μ_{if} is the transition dipole, and t_{21} and t_{32} the time intervals between pump and dump, and dump and probe pulses, respectively. As before, the letters i, j, n, and f refer to the states which are included in the creation of the polarization via the path $|gi\rangle \rightarrow |en\rangle \rightarrow |gj\rangle \rightarrow |ef\rangle$, where g and e refer to the ground and excited electronic states of the species, respectively (see Figure 2.1), and the G-term is defined as in Equation (2.3).

As the signal is detected with a square-law detector by scanning the probe delay t_{23} as explained earlier, the signal is the total polarization squared:

$$\begin{aligned} S &= \int_{-\infty}^{\infty} dT |P^{CARS}(T)|^2 \\ &= \frac{2}{\hbar^6} \sum_{ii',ff',xx'} p_x p_{x'} \int_{-\infty}^{\infty} dT a_{fi}(T) a^*_{f'i'}(T) \mathrm{e}^{-i(\omega_{fi}-\omega_{f'i'})T}. \end{aligned} \tag{2.12}$$

The rapidly oscillating terms (with $\omega_{fi}+\omega_{f'i'}$) have been neglected according to the rotating wave approximation as in Equation (2.6). As the probe delay

t_{32} is scanned, the signal oscillates due to the product of the polarization amplitudes a_{fi} and $a_{f'i'}$:

$$a_{fi}(T)a^*_{f'i'}(T) = \mu_{if}\mu_{i'f'} \sum_{jj',nn'} \mathrm{e}^{-i(\omega_{ji}-\omega_{j'i'})t_{32}} \mathrm{e}^{-i(\omega_{ni}-\omega_{n'i'})t_{21}} \times G_{fjni}(T)G^*_{f'j'n'i'}(T). \quad (2.13)$$

Equation (2.12) is the total signal that can be measured from the sample, and it consists of quantum beats for all the different species in the sample, and, additionally, the polarization beats, that appear in the equation as cross terms with different p_x's. Thus, the polarization beats are an intermolecular interference effect due to the square-law detection of the signal, in contrast to the intramolecular quantum beats.

For a more intuitive presentation, Equation (2.12) can be separated into different terms similarly as was done for Equations (2.7 2.9), to obtain representations for either the quantum beats of the separate species, or the polarization beats. Additionally, the equations can be simplified by assuming that all the molecules are initially on their lowest vibrational state with $v = 0$, which is valid for the low temperatures of the matrix isolation experiments presented in this thesis, and by treating the dump delay t_{12} as constant, as only the probe delay t_{23} is scanned in these experiments. Making these assumptions for a two-species sample, like a matrix with uncomplexed and complexed molecules, these equations become[II]

$$S_F \propto p_F^2\mu_F^2 \sum_{v_F,v'_F} g_{v_F}g_{v'_{F'}} \cos[\omega_{v_F,v'_{F'}}t_{32}]\mathrm{e}^{-(\gamma_{v_F}+\gamma_{v'_F})t_{32}} \quad (2.14)$$

for the quantum beats for the "free" or uncomplexed molecule,

$$S_C \propto p_C^2\mu_C^2 \sum_{v_C,v'_C} g_{v_C}g_{v'_C} \cos[\omega_{v_C,v'_C}t_{32}]\mathrm{e}^{-(\gamma_{v_C}+\gamma_{v'_C})t_{32}} \quad (2.15)$$

for the quantum beats of the complexed molecule, and

$$S_{FC} \propto p_F p_C \mu_F \mu_C \sum_{v_F,v'_C} g_{v_F}g_{v'_C} \cos[(\omega_{v_F,} - \omega_{v'_C,})t_{32}]\mathrm{e}^{-(\gamma_{v_F}+\gamma_{v'_C})t_{32}} \quad (2.16)$$

for the polarization beats between the uncomplexed molecule and the complex. The g_v-terms are the amplitudes of a given vibrational eigenstate v in the superposition, and the subscripts F and C refer to the uncomplexed and complexed molecules, respectively.

In Equations (2.14–2.16), an exponential dephasing term $\mathrm{e}^{-(\gamma_v+\gamma_{v'})t_{32}}$ has also been added, with γ_v representing the dephasing rate for a given

vibrational state v, similarly to Equation (2.9). If there is no correlation between the different species through a common heat-bath mode, the dephasing constant for the polarization beats can be expressed as a sum of the intramolecular dephasing rates of the eigenstates in question, similarly to quantum beats.[135] In the experiments presented in this thesis, the different species are isolated from each other in a solid, low temperature krypton matrix with a high dilution, so the assumption of no correlation between the different species is acceptable and the dephasing times can be written for the polarization beats as in Eq. (2.16).

The effect of polarization beating on the fs-CARS signals can be seen in Figure 2.4. Comparing the Equations (2.14) and (2.15) with Equation (2.16), it is obvious that the polarization beats contain similar information as the quantum beats, for example on vibrational frequencies and dephasing rates of the system. Also, it is important to notice that the amplitude or intensity of a polarization beat is proportional to the product of the weight factors p_F and p_C. If the weight factor of one of the species is smaller than the other's, say $p_F \gg p_C$, the amplitude of a polarization beat, proportional to $p_F p_C$, is notably higher than the amplitude of the respective quantum beat of the species with the weaker signal, that is proportional to p_C^2. As the weight factors are related to the concentrations of the different species, the polarization beats can be used as "amplifiers" for a signal of a small concentration species that might have its quantum beat amplitude below the detection limit.[II,V] This amplification process can be considered as an example of the well known technique of heterodyne detection where a weak signal emitted from a sample is mixed with another, relatively strong field in order to amplify the weak signal.[121] Here, the strong field is generated in the molecule instead of using an external field, but the working principle is identical. The different species may also have different transition dipoles, which has a similar effect on the total signal as the weight factor as can be seen from Eq. (2.16). Thus, the polarization beats can also be used to detect a signal that is weaker due to a smaller transition dipole in a similar way as for the species at low concentration.[IV]

In addition to the amplification effect, polarization beats also help in resolving the bands in fs-CARS spectra of two species that have similar vibrational frequencies. If the vibrational energy level structure of the two species is similar, their quantum beats also appear at similar frequencies, leading to the bands overlapping in the frequency domain spectra. This usually means that the quantum beats of the species with the smaller amplitude are not easily detected even though the amplitude might be above the detection limit in itself. However, the polarization beating leads to new frequency oscillations in the CARS signal, at the difference frequencies of the two different

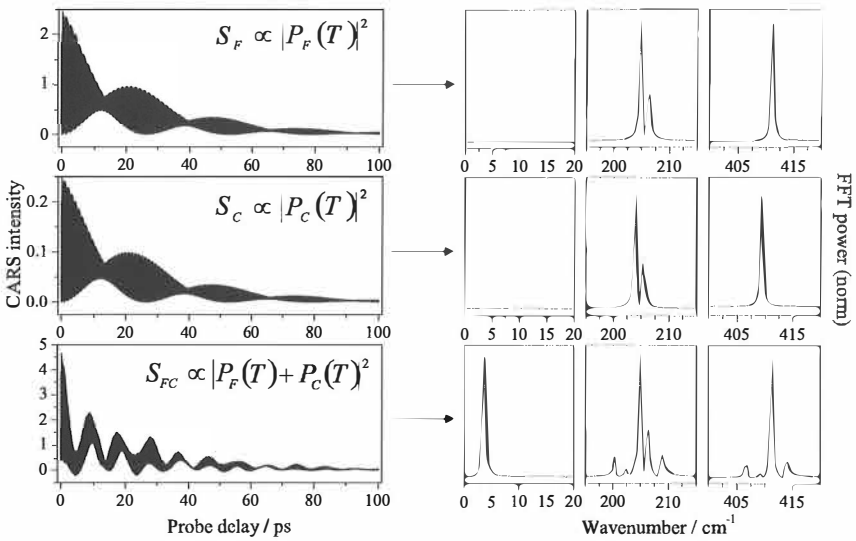

Figure 2.4: A simulation of the creation of polarization beats in the CARS signal in the case of two different species with slightly different vibrational frequencies in the sample. Left: Time-domain CARS spectra. Right: Frequency domain CARS spectra, i.e. Fourier transforms of the time-domain signals. Top row: The stronger signal. Middle row: The weaker signal (note the intensity scales on the left). Bottom: The combined signal. Due to the square-law detection, cross-terms or so called polarization beats are seen in the signal, oscillating with the difference frequencies of the two species. The stronger signal works in the polarization beats as an "amplifier" for the weaker signal, which has no visible quantum beats in the combined signal due to its small intensity. The spectra are simulated using the measured vibrational frequencies and dephasing times of the iodine molecule and the I_2–Xe complex. Intensities in the frequency domain spectra are not comparable as each panel is scaled independently to better show the details.

species of the sample that are usually easier to resolve. This effect is also seen in the simulation in Figure 2.4, with new bands appearing around the quantum beat bands, and at the low frequency domain, where no quantum beats exist. These bands are well resolved from the quantum beats, but still contain the same information on vibrational frequencies and dephasing rates of the species as the quantum beat bands, and are thus helpful in analysing the properties of the system. In this work, the polarization beats are used

for analysis of the data in both "amplification" and resolution enhancement senses.

Polarization beats as a spectroscopic tool for a molecular complex

As can be seen from Equation (2.16), the polarization beats can be used to determine vibrational frequencies, dephasing rates, and relative concentration of the weaker signal species in the sample, provided that these properties are known for the stronger signal species. As in our case $p_F > p_C$, or $p_F^2 > p_F p_C$, the quantum beats of the stronger signal species are always detected, and thus its properties can be determined with relative ease. The polarization beats are then available for the determination of the properties of the weaker signal species.

The first task in analysing the polarization beats is to determine the origin of the polarization beat bands, i.e. to assign the beatings to different eigenstates that are involved in the coherent excitation. In the case of a molecular complex, where the shift in vibrational frequency upon complexation is small, the beatings at the low frequency domain ($< 50\,\mathrm{cm}^{-1}$ in the case of iodine) can be assigned to the polarization beats that oscillate at the difference frequencies of the eigenstates with the same quantum number v in both the complexed and uncomplexed molecule. At the higher frequencies, the oscillations are due to eigenstates that differ with one ($\sim 200\,\mathrm{cm}^{-1}$) or two ($\sim 400\,\mathrm{cm}^{-1}$) vibrational quanta. However, to precisely assign the bands, it is necessary to know whether the vibrational frequencies are red- or blue-shifted upon complexation. This can be determined by inspecting the band positions at the mid-frequency range, where $v_F = v_C \pm 1$. In this case, assuming that the species can be described as Morse oscillators, the band frequencies can be calculated as[II]

$$\omega_{v_F,(v+1)_C} = \nu_{v,(v+1)} + (v+1)(\omega'_e - \omega_e) - (v+1)(v+2)(\omega'_e x'_e - \omega_e x_e) \quad (2.17)$$

and

$$\omega_{(v+1)_F,v_C} = \nu_{v,(v+1)} - v(\omega'_e - \omega_e) + v(v+1)(\omega'_e x'_e - \omega_e x_e), \quad (2.18)$$

where primed symbols refer to the complex, and $\nu_{v,(v+1)}$ is the frequency of the quantum beat of the uncomplexed molecule with the same vibrational level components.

If we further assume that the anharmonicity is approximately the same for both species, the contribution of the anharmonicity to the band position is small and Eqs. (2.17) and (2.18) reduce further to:

$$\omega_{v_F,(v+1)_C} = \nu_{v,(v+1)} + (v+1)\Delta\omega_e \quad (2.19)$$

and

$$\omega_{(v+1)_F,v_C} = \nu_{v,(v+1)} - v\Delta\omega_e\,, \tag{2.20}$$

where, for simplicity, $\omega_e' - \omega_e = \Delta\omega_e$. If the complex is red-shifted, $\Delta\omega_e < 0$, the polarization beat band to the red from the corresponding uncomplexed molecule's quantum beat band, $\omega_{v_{I'},(v+1)_C}$, should be farther off from that quantum beat band by $\Delta\omega_e$, when compared to the polarization beat band on the blue side of the uncomplexed molecule's quantum beat band, $\omega_{(v+1)_F,v_C}$. However, if the complex is blue-shifted, $\Delta\omega_e > 0$, the situation is turned around so that the polarization beat band closer to the corresponding uncomplexed molecule's quantum beat band is now to the red from it. In Figure 2.5, the assignment is demonstrated for the red-shifted case of the I_2–Xe complex.

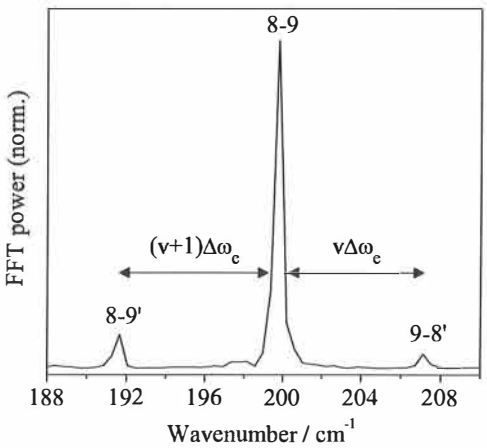

Figure 2.5: Demonstration of the use of Equations (2.19–2.20) in assigning the direction of the shift in the complexed molecule. The polarization beat band (8-9') to the red from the corresponding quantum beat band (8-9) is farther off from the quantum beat band than the polarization beat band on the blue side of the quantum beat (9-8'). Thus, the iodine vibrational frequency is red-shifted upon complexation. The spectrum is measured for the v = 8-9 wavepacket in the I_2/Xe/Kr sample at $T = 4.1$ K.[II]

After assigning the bands in the spectra, Morse parameters for both the free and complexed molecule can be determined. For the uncomplexed molecule's quantum beat bands, with frequencies of $\omega_{(v+1)_{I'}} - \omega_{v_{I'}}$, normal

Birge-Sponer analysis can be performed by a linear fit to the band positions,

$$\omega_{(v+1)_F} - \omega_{v_F} = \omega_e - 2\omega_e x_e(v_F + 1). \tag{2.21}$$

To find Morse parameters for the complexed molecule, the polarization beat frequencies can be used, if its quantum beats are not visible in the spectra. The polarization beat bands appear at the frequencies of $|\omega_{v_F,0} - \omega_{v_C,0}|$. The $\omega_{v_F,0}$ terms can be calculated from the uncomplexed molecule's Morse parameters determined from its quantum beats, allowing the calculation of the $\omega_{v_C,0}$ terms from the polarization beat frequencies. A linear fit of the function

$$(\omega_{v_C} - \omega_0)/v_C = \omega'_e - \omega'_e x'_e(v_C + 1) \tag{2.22}$$

can then be used to determine the Morse parameters for the complexed molecule.

The determination of the dephasing rates from the polarization beats for the weaker signal species is straightforward, after the dephasing rates for the stronger signal species have been determined from its quantum beats. According to Equation (2.16) the bandwidths of the polarization beat bands in the frequency domain are proportional to $(\gamma_{v_F} + \gamma_{v'_C})$, and as γ_{v_F} can be obtained from the quantum beats, the determination of $\gamma_{v'_C}$ is only a matter of simple calculation.

To estimate the relative concentration of the complex in the sample, the intensity of the polarization and quantum beat bands with same vibrational components can be used, as implied by Eqs. (2.14) and (2.16):

$$\frac{\mathrm{A}_{FC}(v_F,v'_C)}{\mathrm{A}_F(v_F,v'_F)} \quad \frac{p_F p_C \mu_F \mu_C y_{v_F} y_{v'_C}}{p_F^2 \mu_F^2 g_{v_F} g_{v'_F}}, \tag{2.23}$$

where A_F is the amplitude of the quantum beat band of the uncomplexed molecule, and A_{FC} the amplitude of the corresponding quantum beat band ($v'_C = v'_F$). For a broadband excitation of two species that have similar vibrational level structures, Equation (2.23) can be simplified by estimating that the wavepacket weights g_v for the uncomplexed and complexed molecule are roughly the same, $g_{v'_C} \approx g_{v'_F}$, i.e. the amplitude of a certain eigenstate in the wavepacket is similar for both the complex and the uncomplexed molecule. However, this approximation becomes more inaccurate for higher vibrational wavepackets, as the difference in the vibrational level energies between these two species grows larger. To compare only the concentrations, it is also necessary to make an approximation of $\mu_C \approx \mu_F$, which implies that the electronic states of the molecule should not be significantly modified upon complexation. After these approximations, Eq. (2.23) reduces to

$$\frac{\mathrm{A}_{FC}(v_F,v'_C)}{\mathrm{A}_F(v_F,v'_F)} \quad \frac{p_C}{p_F}, \tag{2.24}$$

and the relative concentration of the complex compared to the uncomplexed molecule can be estimated. Evidently, if it was possible to determine the concentrations of the different species using a different method, the intensities of the bands could also be used in a similar way to estimate the relative transition dipoles, μ_C/μ_F, for the two species.

In the case where the two species contributing to the polarization beats are not a molecule and its complex, many of the approximations mentioned above cannot be safely made. For example, $\mu_C \neq \mu_F$, and as the vibrational energy level structures of the molecules are totally different, $g_{v'_C} \neq g_{v'_{I'}}$. In this case, the assignment of the polarization beat bands has to be done with care, estimating which vibrational levels of the different molecules can be excited with the pump-dump-process, and using the observed quantum beats as a help. After assignment, the vibrational analysis and the determination of dephasing rates can be done in a way similar to the one presented here.[IV]

2.3 Experimental setup

The experimental setup used in this work consists mainly of a liquid helium flow cryostat (Janis Research Co.) with a vacuum gas line attached for sample preparation, combined to a femtosecond CARS setup. UV-vis and resonance Raman spectra were measured using the same cryostat and self-made spectrometers, but for the FTIR measurements the cryostat was changed to a closed-cycle system (APD Cryogenics HC-2), integrated with a commercial FTIR spectrometer (Nicolet Magna-IR 760 ESP). The frequency scales for the resonance Raman spectra were calibrated using the vibrational frequencies of the uncomplexed iodine molecule in solid Kr, obtained with high accuracy from the fs-CARS measurements.

The samples were prepared by mixing proper partial pressures of the sample gases, iodine and krypton, with xenon or benzene when applicable, in a gas bulb in a vacuum line. The I_2/Kr ratio, 1/2600, was kept constant throughout the experiments, as it was found that with this dilution the iodine in the sample stays monomeric and no detectable amounts of dimers or higher order clusters are present. The amount of xenon or benzene in the sample was varied during the experiments to optimize the concentration of the 1:1 complex without significantly increasing the amount of higher clusters. The solid matrices were then prepared by slowly spraying the gas mixture on a $\sim 100\,\mu$m thick sapphire window kept at $T = 40$ K, except for the IR measurements, where a CaF_2 window was used to allow transmission of the IR wavelengths. The matrix preparation method was studied carefully before starting the actual measurements to obtain best possible matrices with

known thickness, high optical quality and monomeric samples.[I] When lowering the temperature, slow cooling rate of $\sim 0.5\,\mathrm{K/min}$ was used in order to minimize the damage to the matrix. The cryostat was equipped with an external mechanical pump in order to enable cooling down to $T = 2.6$ K, but mainly temperatures between 10–40 K were studied because of the unavoidable deterioration of the matrix quality at the lower temperatures due to cracking.

Schematic presentation of the fs-CARS setup is shown in Figure 2.6. In the course of the work presented in this thesis, two different femtosecond setups were used, but the actual working principle is similar in both. An oscillator-amplifier system (either Coherent Mira + Quantronix Odin or Coherent Libra) was used to generate short laser pulses with $\lambda_{max} \sim 800\,\mathrm{nm}$, pulse length of $\sim 100\,\mathrm{fs}$, and repetition rate of 1 kHz. From this, two or three different wavelength pulses, depending on the experiment, were generated using optical parametric amplifiers (OPA's);[122] either self made non-collinear optical parametric amplifiers (NOPA's)[II,IV,V] or a commercial OPA (Topas, Light Conversion Ltd.).[I] In the case of two-color experiments, one of the pulses was splitted into pump and probe pulses, whereas the other pulse was used as the dump pulse. In three-color experiments, each pulse was of different wavelength. Three delay lines were used in the experiment to allow easy adjustment of the timing of the pulses, and neutral density filters were used to control the intensity of the pulses at the sample. The pulses were arranged in a boxcar geometry as in Figure 2.2, and the CARS signal, emitted in the $\mathbf{k}_{pump}$ $\mathbf{k}_{dump}$ | $\mathbf{k}_{probe}$ direction, was filtered through an aperture, an interference filter, and a monochromator to a photomultiplier tube (PMT). The signal was collected with a boxcar integrator with a step size of the probe delay line of 6.7–20 fs, and 300–1000 pulses were averaged for one data point.

Even though generating three colours instead of two slightly complicates the experiment, it also proved useful as the samples were somewhat scattering. In two-color experiment, the signal emitted to the $2 \times \mathbf{k}_{pump} - \mathbf{k}_{dump}$ direction, also generated in the sample, is of the same wavelength as the CARS signal, emitted in $\mathbf{k}_{pump} - \mathbf{k}_{dump} + \mathbf{k}_{probe}$ direction. In a solid matrix sample, the signals are scattered and totally eliminating the $2 \times \mathbf{k}_{pump} - \mathbf{k}_{dump}$ signal from the measured signal is difficult, generating a disturbing background. In a three-color experiment, these two signals occur at different wavelengths, and thus a narrow-band interference filter can be used to eliminate this disturbance. Also, as the signal has to be filtered spectrally, the three-color experiment allows for more flexibility in choosing the wavelengths used to generate a desired wavepacket, as in practice there is only a limited selection of interference filters in the laboratory.

Both the spatial and temporal overlap of the three fs-laser pulses was

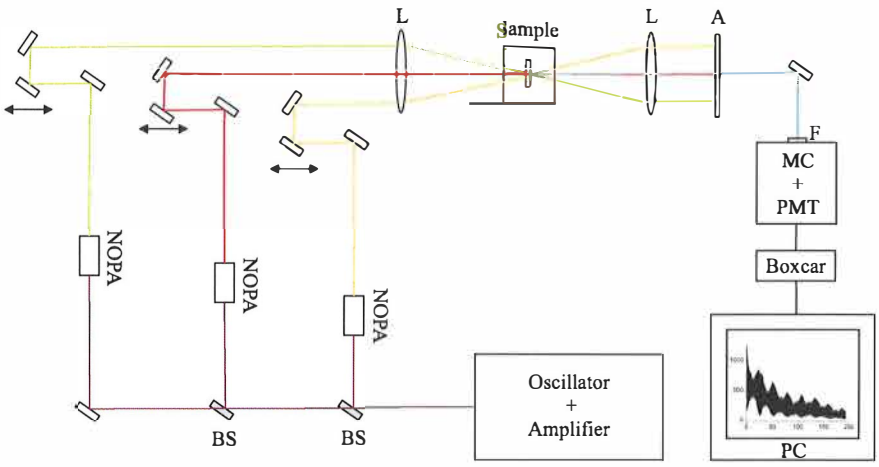

Figure 2.6: Schematic presentation of the setup for the fs-CARS experiments. The 800 nm output of the femtosecond laser system is used to generate up to three different colours in optical parametric amplifiers to obtain three laser pulse beams necessary for the CARS experiment. All three laser lines are equipped with a delay line to allow easy adjustment of the timing of the pulses. The three beams are arranged in the boxcars geometry (Fig. 2.2), and the CARS signal is filtered through an aperture (A), interference filter (F), and a monochromator (MC), and detected with a cooled photomultiplier tube (PMT). The PMT signal is collected with a boxcar integrator as a function of the probe delay.

adjusted using a BBO crystal to obtain a visible CARS signal at so called zero-delay, where all the pulses are overlapped in time. After confirming the overlaps, the sample was put in place of the BBO crystal and the CARS signal was re-optimized. The optimization included adjusting the time delay between pump and dump pulses, which changes the time the wavepacket spends on the excited electronic state before the dump transition. This adjustment optimizes the CARS process so that the dump transition takes place at the Franck-Condon region favorable for the vibrational wavepacket that is generated in the experiment in question, similarly to the $(TD)^2$CARS scheme by Knopp *et al.*[59,60,87]

After optimization, the fs-CARS signal was measured keeping the pump-dump delay constant, and changing the probe delay. Usually, the step size Δt was 20 fs, as shorter steps would only lengthen the measurement time

but would not give any extra information, as the highest iodine vibration frequencies are well below the highest frequency that can be observed (Ω_{max}) according to the Nyquist theorem; $\Omega_{max} = \pi/\Delta t$.[16] The signal was measured as long as oscillations were visible; typically for probe delay of 30–200 ps, depending on the temperature and wavepacket composition. The measurement was then repeated similarly at different temperatures. The frequency domain spectra, revealing the oscillation frequencies in the CARS signal, were obtained by Fourier transforming the corresponding measured time domain signals.

3 Results and discussion

The purpose of the work presented in this thesis was to study the vibrational coherence on the ground electronic state of the iodine molecule and its complexes isolated in a solid krypton environment. The temperature- and vibrational state dependence of the dephasing rate was studied to find out the nature of the interactions in the system. Then, the properties of the different complexes were determined using various spectroscopic methods to obtain detailed information on their structures, vibrational energies, and coherence lifetimes. Finally, highly excited vibrational wavepackets were prepared when possible, to study the possibility to use them in the final goal of using the ground electronic state vibrations as a starting point in controlling a bimolecular chemical reaction. This chapter summarizes the most important results, and discusses the conclusions that can be made from the results concerning the coherent control of the reactions of these systems. The details of the studies are presented in Papers I–V.

3.1 Iodine molecule in solid krypton

The monomeric iodine molecule isolated in a solid krypton matrix was studied using fs-CARS technique as described in Section 2.3 (Paper I). The fs-CARS signals were measured for four different superpositions, and five different temperatures between 2.6–32 K to find out the temperature- and vibrational state dependence of the dephasing rates. The signals reveal the quantum beating of the iodine molecule as oscillations with the difference frequencies of the different vibrational levels, as explained in section 2.2.

The measurements, shown in Figure 3.1 for $T = 20$ K, reveal that the dephasing times for monomeric iodine isolated in low-temperature solid krypton matrix are long, with the signal being detectable even for probe delays of over 200 ps for the lowest vibrational states. The vibrational state dependence of the dephasing rate is clear even from Figure 3.1, but the temperature dependence was found to be weaker. The long dephasing times result in narrow bands in the frequency domain spectra, but as the dephasing

times shorten with the increasing vibrational quantum number v, the bands also start to overlap in the frequency domain for the higher states.

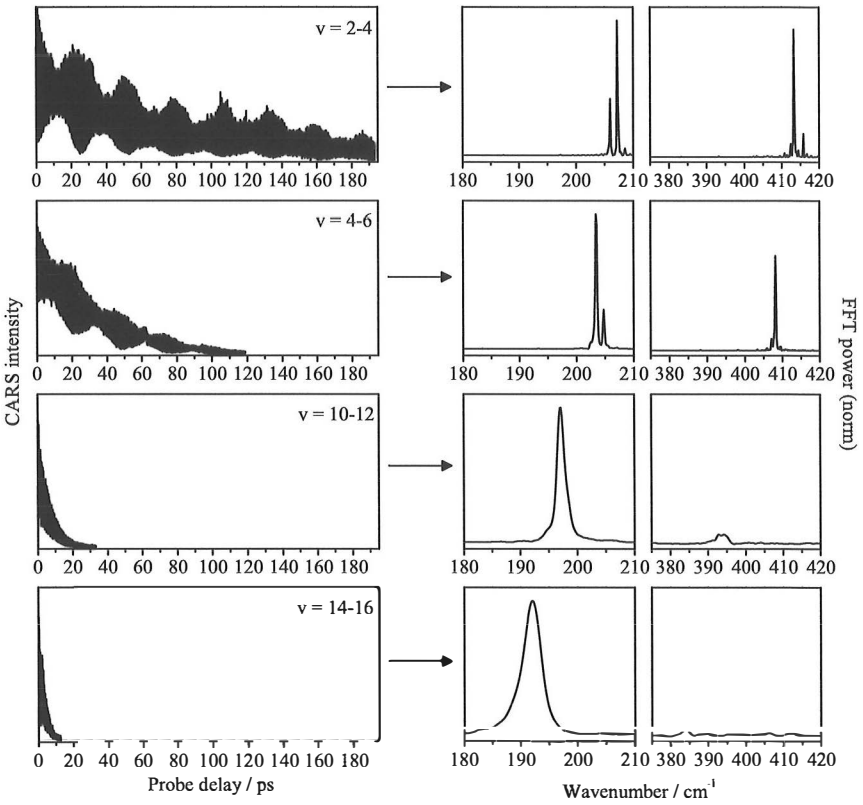

Figure 3.1: Fs-CARS spectra for monomeric iodine in solid krypton at $T = 20$ K for different wavepackets. Left: time-domain signals. The time scale is the same for all measurements to emphasize the change in dephasing time as a function of vibrational state. Right: FFT of time domain signals, i.e. the frequency domain spectra. The same wavenumber scale on the vertical rows of panels shows how the oscillation frequency changes and the bands widen as the vibrational quantum number increases. The intensities of the bands are not comparable between the right and left frequency domain panels as the scale has been changed to show the details.

From the fs-CARS spectra, the vibrational frequency of the iodine molecule in solid krypton was determined using the Birge-Sponer analysis (Eq. (2.21)), yielding $\omega_e = 211.20 \pm 0.01\,\mathrm{cm}^{-1}$ and $\omega_e x_e = 0.642 \pm 0.001\,\mathrm{cm}^{-1}$ at $T = 32$ K. The value of ω_e is notably smaller than the value found in the previous studies by Karavitis *et al.*,[70,71] but the variation can be explained by the differences in the sample morphologies due to different preparation methods.

The dephasing rates γ_v were determined from fits of both time and frequency domain spectra, and the results from both were in good agreement. The accuracy of the results decreased with increasing v, as the frequency domain bands started to overlap. However, a clear temperature- and v-dependence were found for the dephasing rates for the $v = 2$–15 and $T = 4.1$–32 K range. At $T = 2.6$ K, the dephasing rate of the lowest vibrational states was found to increase when compared to 4.1 K, which is interpreted as an inhomogeneous contribution due to the strains created in the matrix during cooling below 4.1 K, visible also to the eye as crack formation and increased light scattering in the sample. Thus, the 2.6 K data for these states were excluded from the analysis. Both the T- and v-dependence of the dephasing rate were analysed by fitting the data with equations for an impurity in a solid lattice in a weak coupling limit by Skinner *et al.*.[70,125,127] The weak temperature dependence and the roughly quadratic v-dependence found indicate that the main dephasing mechanism is coupling to pseudolocal phonons with a frequency of $\sim 34\,\mathrm{cm}^{-1}$. The contribution of vibrational relaxation and inhomogeneous broadening, dictating the lower limit of the dephasing rate as $T \to 0$, could not be determined from the data. As the longest coherence times were up to hundreds of picoseconds, there might be a contribution from the vibrational lifetime in the obtained values.

The high spectral resolution of the measurement also allowed the detection of a temperature dependent frequency shift for the $v = 2$–4 bands. The $\omega_{2,3}$ band shifts to lower frequencies only $\sim 0.14\,\mathrm{cm}^{-1}$ when going from 32 to 4.1 K, but the shift is still well detectable. The line shift, like the dephasing rate, is also a measure of the interactions between the molecule and its environment.[125,127] A fit to the experimental data supports coupling to pseudolocal phonons with a frequency of $\sim 23\,\mathrm{cm}^{-1}$, in reasonable agreement with the analysis of the dephasing rates.

As a conclusion, the fs-CARS method was found to be succesful in preparing and interrogating vibrational wavepackets on the ground electronic state of the iodine molecule isolated in solid krypton matrix, and the data obtained could be used to determine the properties of the system, and the nature of the couplings between the molecule and its environment. The long dephasing times allow the following of the evolution of the wavepacket for

hundreds of vibrational periods, and obtaining data on the system with high accuracy.

3.2 Iodine-xenon complex

The study of iodine vibrations was extended to cover effects upon complexation with different species. The first species studied was a weak complex between the iodine molecule and the xenon atom, considered in Papers II and V. The I_2–Xe system has already been considered as a model system for reaction control experiments.[31,32] It is also simple to prepare and analyze experimentally, and to model computationally. The goal was to investigate the properties of the complex, and to see how the complexation affects the dephasing rate of the iodine vibrations on the ground electronic state. Finally, high vibrational states were excited in the complex, to probe the high energy regions of the ground state potential, and to estimate the usefulness of the complex system as a model for bimolecular reaction control.

In the I_2/Xe/Kr samples, there are always both uncomplexed iodine molecules and I_2–Xe complexes present. Thus, the fs-CARS signal consists of signals of two different species, and polarization beats are detected. In fact, in the experiments presented here, the concentration of the complex was so low that the quantum beats of the complex were not visible, and the polarization beats were used to analyze the properties of the complex as explained in Section 2.2.1. The monomeric, uncomplexed iodine, present in samples in significant amounts, was thus used as an "amplifier" for the complex signal. Also, as was found from the analysis, the shift in the vibrational frequency upon complexation is so small that the quantum beats of the complex, even if more intensive, would have been overlapped by the uncomplexed iodine signal, so the polarization beats were also useful from the resolution point of view.

The fs-CARS signal is shown for two different wavepackets in Figure 3.2. The excitation of very high vibrational states succeeded for the complex, with $v_{max} = 22$. The strongest bands in the spectra in Figure 3.2 are quantum beats of the uncomplexed iodine, and polarization beats can be seen on both sides of the quantum beats, and at the low frequency region, where no quantum beats exist. Using Equations (2.17–2.22), the I_2–Xe complex vibrations were found to be redshifted by 0.90 cm^{-1} when compared to the uncomplexed iodine molecule in krypton, with $\omega'_e = 210.36 \pm 0.04\,cm^{-1}$ and $\omega'_e x'_e = 0.636 \pm 0.003\,cm^{-1}$ for the complex at $T = 10$ K. The vibrational analysis for the uncomplexed iodine molecule gives within the error limits the same result as from the sample with plain monomeric iodine, showing

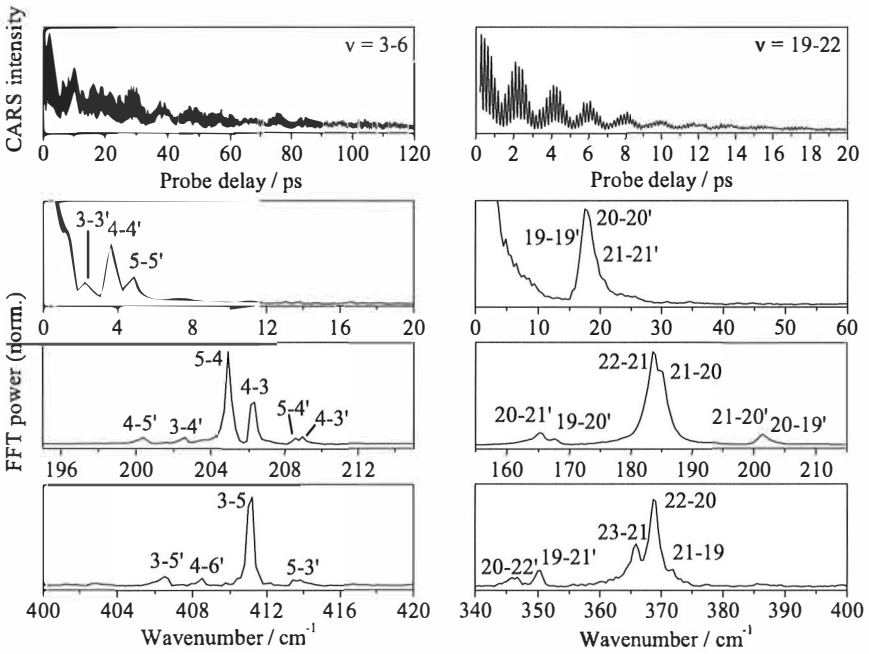

Figure 3.2: Fs-CARS spectra for I_2/Xe/Kr sample at $T = 10$ K for wavepackets with $v = 3$–5 (left) and 19–22 (right) in both time and frequency domain, showing quantum beats for uncomplexed iodine, and polarization beats between the complexed and uncomplexed iodine. Polarization beating is visible in the time domain spectra as a more complex oscillatory structure than for the plain iodine-krypton samples (Fig. 3.1). The bands are labelled similarly as in Figure 2.3, with primed numbers referring to the vibrational states of the complexed iodine molecule, and the numbers without primes to the states of the uncomplexed molecule. The intensities of the bands are not comparable between the different frequency domain panels as the scale has been changed to better show the details. Note also the different wavenumber and delay scales of the left and right spectra.

that adding xenon to the sample does not noticeably change the morphology of the sample. No quantum beating was observed for the complex, which is understandable due to the small shift in vibrational frequency, leading to overlap with the uncomplexed iodine quantum beats. Additionally, using Equation (2.24), the complex/iodine ratio p_C/p_F was estimated to be $\sim 1/3$,

so the intensity of the complex quantum beats was also too low to be well detected.

From the polarization beats, the dephasing rates for the vibrations of the complexed iodine molecule on its ground electronic state were also determined.[II,V] For the higher vibrational states, the bands are broad and overlapping, so the results are not the most accurate, but the rates were found to be slightly higher for the complex, with a similar v-state dependence as for the monomeric iodine. Thus, the weak complexation does not change the dephasing mechanism but only makes the dephasing slightly faster. The temperature dependence of the dephasing rates was weak for the complex, similarly to the uncomplexed molecule. Thus, the results for the complex indicate dephasing via pseudolocal phonons as for the uncomplexed molecule.[I,70]

To find the structure of the complex, experimental vibrational frequencies for the complex were compared with computational results for several different structures.[II] As the fs-CARS spectra clearly indicate a redshift in the complexed iodine's vibrational frequency, the calculated structures with a redshift in the iodine vibrational frequency were selected for further comparison. Of these, the structure with the lowest energy, the linear "head-on" complex (Figure 3.3) was selected as the most probable. Although it might be possible to have several different conformations of the complex in the same sample, the spectrum does not indicate more than two species in the sample. Should other structures exist, their concentrations are much lower so that even the polarization beats are not detected. Additional computational methods were used to simulate the fs-CARS spectra to confirm our assignment of the quantum- and polarization beats.

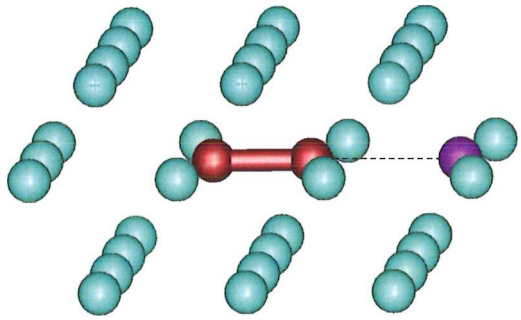

Figure 3.3: The most probable structure of the I_2–Xe complex isolated in solid krypton (matrix cage atoms depicted in turquoise), obtained by comparing experimental and computational results.[II]

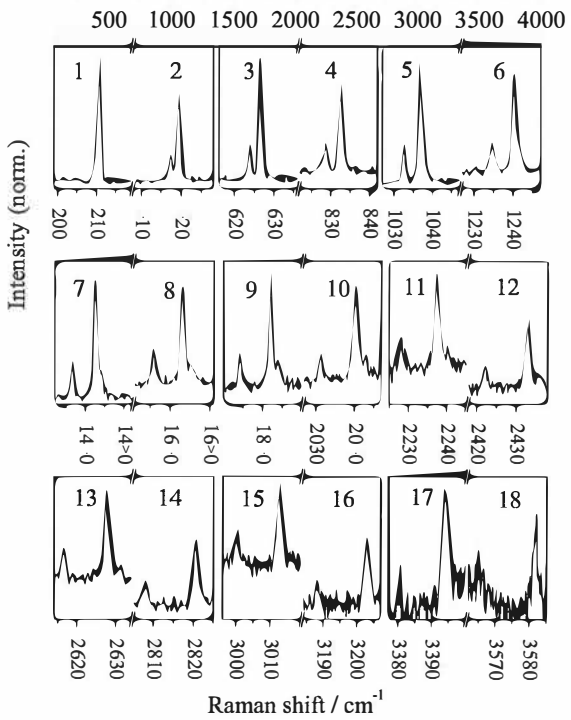

Figure 3.4: Resonance Raman spectrum for the I_2/Xe/Kr sample at $T = 10$ K showing the vibrational progression for both complexed and uncomplexed iodine. Upper panel: A lower resolution ($\sim 5\,\mathrm{cm}^{-1}$) spectrum showing the progression up to $v = 20$. The spectrum is generated by combining the results of two measurements. The narrow Raman bands ride on a background of hot luminescence and fluorescence.[49] Lower panels: Higher resolution ($\sim 1\,\mathrm{cm}^{-1}$) spectrum showing the well separated bands of both the uncomplexed iodine (higher frequency and intensity) and the I_2–Xe complex (lower frequency and intensity). The bands are labelled according to the final vibrational state quantum numbers v of the Raman transitions. The intensities of the bands are not comparable between the different panels as the scale has been changed to better show the features of the weaker bands.

The I_2–Xe complex was also studied using spontaneous resonance Raman spectroscopy, as shown in Figure 3.4.[V] High vibrational states, here up to $v = 20$, can also be excited with this method due to the resonance condition, but as the resolution of the method is not as good as with fs-CARS, the bandwidths are instrument limited and the true dephasing rates cannot be obtained. However, the vibrational analysis and the estimation of the upper limits of dephasing rates from the higher resolution spectra agree with the results from the fs-CARS measurements. Also, the relative decrease in the band intensities with the increasing vibrational quantum number was found to be similar for both species, indicating similar excited state dynamics for both.[49]

The results for the I_2–Xe complex show, that the high vibrational states can be excited with a good efficiency also in the complexed iodine molecule. The polarization beating was shown to be a useful phenomenon that can be used to study the properties of a low concentration complex species. The vibrational frequencies, dephasing rates and relative concentration of the complex were analyzed using the polarization beats, and the most probable structure of the complex was determined by comparing this information with the computational results. With the fs-CARS method, high vibrational wavepackets of the complex were excited and interrogated, promising a possibility to control the reactions of the complex using the ground electronic state vibrations as a starting point, as will be discussed in Section 3.4.

3.3 Iodine-benzene complex

The second complex studied in this work was the benzene-iodine complex, which is an extensively studied species, mostly due to its low-lying charge-transfer state.[99–115,136] Our interest in this complex was based on the idea of controlling the charge-transfer reaction by exciting the complex on different reactive or unreactive potential surfaces, similarly as for the I_2–Xe complex. However, unlike the xenon complex, the I_2–Bz complex allows to extend the studies to room temperature liquid and gas phases. In Papers III and IV, the properties and structure of the complex isolated in solid krypton were studied, paying specific attention to the vibrations of the iodine molecule on the ground electronic state, using resonance Raman scattering, FTIR and UV-vis absorption, and fs-CARS techniques.

The structure of the 1:1 I_2–Bz complex was confirmed experimentally using FTIR spectroscopy. Several calculations had already suggested the structure of the complex to be unsymmetric with the iodine molecule located almost perpendicularly above a C–C bond or a C atom of the benzene

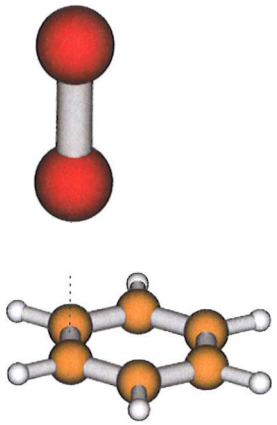

Figure 3.5: Computationally obtained[III] above-bond type of structure for the I_2–Bz complex, which was confirmed to be the ground state structure by the measurements presented in this thesis.

ring,[101,103,104,III] but no direct experimental evidence on this kind of ground state structure was reported at the time of this work. The matrix isolation FTIR data in this work,[III] however, revealed splittings in the vibrational bands that are degenerate for benzene and the symmetric complex (C_{6v}), indicating an unsymmetric, above-bond structure (C_s, Figure 3.5) that is also supported by several computational results.

In the UV-vis measurements, the B←X absorption of the iodine molecule was found to be blue-shifted $\sim$ 25 nm upon complexation with one benzene molecule. This kind of environmentally induced blue shift has also been detected earlier in several environments, from different solvents[100] to clathrate hydrate cages,[137] and is due to the relative energetic stabilization of the ground state of iodine compared to the upper state. Interestingly, this shift is similar to the shift detected when going from a gas phase iodine molecule to iodine in benzene solution ($\sim$ 30 nm),[100,138] suggesting that also in liquid benzene, iodine is on average mainly complexed with only one benzene molecule.

Spectroscopic parameters for the iodine molecule in an iodine-benzene complex were analyzed from the resonance Raman spectrum (Figure 3.6), where the vibrational progression for both uncomplexed and complexed iodine is clearly visible. The Birge-Sponer analysis of the spectrum yields

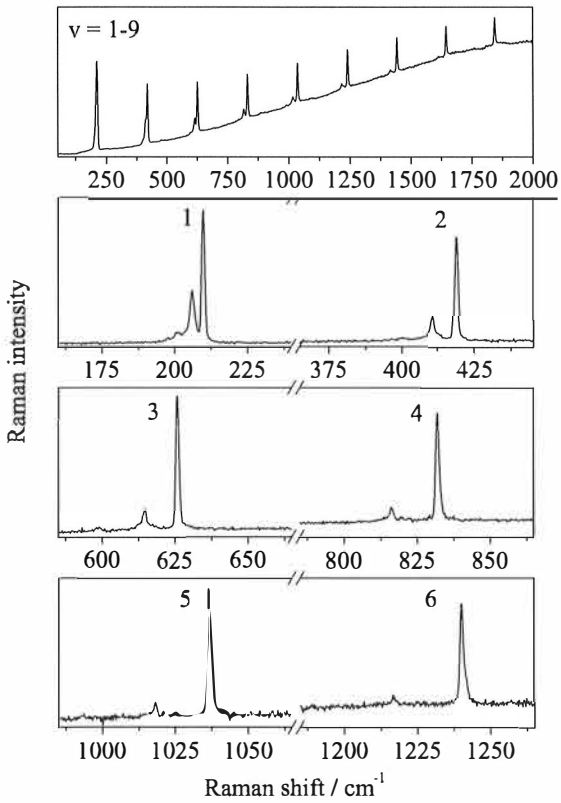

Figure 3.6: Resonance Raman spectrum for I_2/Bz/Kr sample at $T = 30$ K showing the vibrational progression for both complexed and uncomplexed iodine. Upper panel: A lower resolution ($\sim 5\,\mathrm{cm}^{-1}$) spectrum showing the iodine vibrational progression up to $v = 9$. Lower panels: Higher resolution ($\sim 1\,\mathrm{cm}^{-1}$) spectrum showing the well separated bands of both uncomplexed iodine (higher frequency and intensity) and the I_2–Bz complex (lower frequency and intensity), and the faster decay of the complex band intensities with increasing v. The bands are labelled according to the final vibrational state quantum numbers v of the Raman transitions. The intensities of the bands are not comparable between the different panels as each panel is scaled independently to better show the features of the bands.

$\omega'_e = 207.22 \pm 0.07\,\mathrm{cm}^{-1}$ and $\omega'_e x'_e = 0.612 \pm 0.015\,\mathrm{cm}^{-1}$ for the complex. Upon complexation, the harmonic frequency of the iodine vibration is thus red-shifted by $3.94\,\mathrm{cm}^{-1}$, and the anharmonicity constant is slightly reduced. The intensities of the complex Raman bands can be seen to decay faster as a function of v than the uncomplexed iodine bands, indicating different dynamics on the excited electronic state of the systems, i.e. faster electronic dephasing on the B state of the complex.[49,IV] Unfortunately, the widths of the Raman bands measured were instrument limited, and accurate dephasing rates could not be determined from the Raman spectrum. However, the lower limit for the dephasing time could be estimated to be ~ 10 ps for the states $v = 1$–8 that were observed, indicating a weak coupling of iodine with the benzene molecule in the complex.

In the fs-CARS spectrum, polarization beats were detected when exciting the $v = 4$–7 wavepacket of uncomplexed iodine, as shown in Figure 3.7. However, a detailed analysis revealed, that the polarization beating is due to the interference between signals from uncomplexed iodine and uncomplexed benzene molecules, and not from the complexed iodine molecules. In addition to the iodine vibrations, the pump-dump sequence excites the strongly Raman active ring stretch vibration of benzene (ν_2, $\sim 994\,\mathrm{cm}^{-1}$), which causes the interference in the signal. Measurements with different wavelengths that were not exciting any benzene vibrations, revealed only quantum beating of uncomplexed iodine, and no signal from the I_2–Bz complex was detected. However, these results are interesting, because here the strong signal of the uncomplexed iodine molecule functions in the polarization beats as an "amplifier" for an electronically nonresonant, and thus weak benzene signal.

In Figure 3.7, the polarization beating is seen to disappear rather fast in ~ 15 ps, while the quantum beating of iodine survives for more than 100 ps. This is due to the faster dephasing of the benzene ν_2 vibration, for which the dephasing time can be estimated to be ~ 6 ps. The frequency shift upon complexation for the benzene ν_2 vibration was found to be $-3\,\mathrm{cm}^{-1}$, when compared to the frequency of the same vibration of the uncomplexed molecule in krypton matrix. The ν_2 vibration becomes weakly IR active upon complexation, so the complex frequency was determined from the FTIR measurements, whereas the uncomplexed benzene frequency was found from the polarization beats in the fs-CARS spectra.

The reason for not detecting a signal from the I_2–Bz complex is not altogether clear, as the UV-vis, Raman, and FTIR spectra clearly indicate that the complex is present in the sample. The CARS process is also electronically resonant for the I_2–Bz complex, just as for the uncomplexed iodine, meaning that the signal should not be extremely weak in itself. The small concentration of the complex should not be a problem, as the polarization

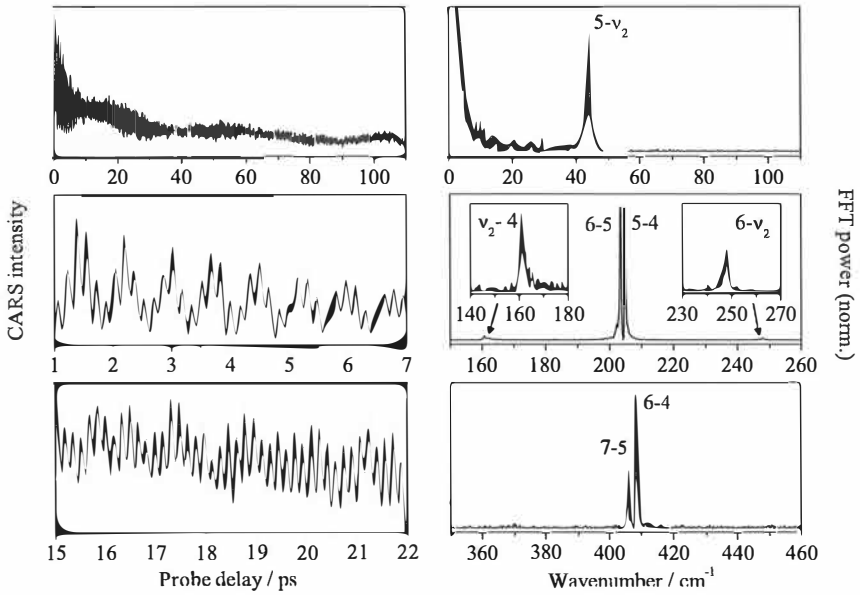

Figure 3.7: Fs-CARS spectra for I_2/Bz/Kr sample at $T = 10$ K for wavepacket with $v = 4$–7 in iodine, in time (left) and frequency (right) domain, showing quantum beats for uncomplexed iodine, and polarization beats between the uncomplexed benzene and uncomplexed iodine molecules. No signal from the iodine-benzene complex is visible in the spectra. Polarization beating in the time domain spectrum is rather short-lived due to the fast dephasing of the benzene vibrations, as can be seen from the lower left panels. In the band labels, ν_2 refers to the benzene ring stretch vibration, and the numbers to the different vibrational states of uncomplexed iodine molecule. The intensities of the bands are not comparable between the different frequency domain panels as the scale is different for different panels to better show the details.

beats should also work as "amplifiers" for this signal, similarly as in the I_2–Xe case. The most plausible explanation for the lacking signal is thus another optical process competing with the fs-CARS process, that could weaken the CARS signal below the detection limit. One possible process could be a two-photon absorption to the charge-transfer state of the complex, which is located at roughly twice the energy of the B←X transition, that gives the resonance condition for the CARS and Raman processes. Thus, chang-

ing the pump wavelengths out of the two-photon absorption resonance would also mean that the resonance condition for fs-CARS would be lost, weakening the uncomplexed iodine signal too. Because of these difficulties, the fs-CARS measurements were not continued for the I_2–Bz complex in the course of the work presented here, but should the nonresonant fs-CARS signal be strong enough for the uncomplexed iodine, the change of the pump wavelengths might clarify the reasons for the loss of the complex signal.

Although the fs-CARS measurements were not succesful for the I_2–Bz complex, they showed that the polarization beating phenomenon can be used to also detect and characterize molecules that are not electronically resonant with the exciting light wavelengths. In addition, the other spectroscopic methods used gave a lot of new information on the I_2–Bz complex. The structure was experimentally confirmed to be of above-bond type using FTIR spectroscopy, and by comparing the results with computational structures. The change in the vibrational frequency of iodine molecule upon complexation was determined using resonance Raman spectroscopy, and the dephasing times for the iodine vibrations were estimated to be longer than ~ 10 ps for the states with $v = 1$–8. The indications of these results on the possibility to control the charge-transfer reaction of the complex using the ground state vibrations as the starting point will be discussed in the next section.

3.4 Prospects of coherent control

The capability of manipulating the vibrations of a molecule or a molecular complex using a designed sequence of short optical pulses opens up possibilities to control the time evolution of a system, and even to manipulate chemical reactions. In the course of this work, an idea of controlling the reactions of the studied complexes using the fs-CARS method emerged.[IV,V] The 1:1 complexes isolated in solid krypton environment can be considered simple, well-defined model systems. Isolating the system in a solid matrix restricts interactions with other complexes, collisions, and diffusion that might complicate the interpretation of the results, and keeps the species taking part in the reaction in the close vicinity of each other. In this section, the possibility of using the ground electronic state vibrations, excited by the pump-dump part of the CARS cycle, as a starting point in controlling a bimolecular charge-transfer reaction is evaluated for the two complexes studied according to the experimental results presented earlier.

3.4.1 The reaction control scheme

The concept of the control process that is evaluated here was introduced and studied theoretically by Tannor, Kosloff, and Rice.[16–18] The basic idea is to use short laser pulses to create a wavepacket that is left to evolve until it reaches a conformation, or a position on the molecular potential, suitable for the reaction. At the right moment, an additional short laser pulse is used to excite the system on another, reactive potential surface in a controlled way, so that the reaction will proceed as desired. The evolving wavepacket can be in principle generated on any potential surface that is deemed useful, with as many laser pulses as necessary.

A simple presentation of the proposed scheme of using the fs-CARS process for the reaction control is shown in Figure 3.8. The pump-dump process is used to generate an evolving wavepacket on the ground electronic state of the system. The properties of the wavepacket can be manipulated by changing the pulse properties. Then, after a proper time of evolution, when the wavepacket has reached the right shape and position on the ground state potential, a third pulse is used to excite the wavepacket to the reactive surface, here the charge-transfer state. Depending on the wavepacket composition and the time delay between the dump and pump pulses, the position or conformation at which the wavepacket reaches the charge-transfer state can be controlled. For example, in Figure 3.8, a direct Franck-Condon excitation to the charge-transfer state from the lowest vibrational states would lead to a repulsive potential and fast predissociation. However, should the excitation happen after the evolution of a wavepacket on the higher vibrational states on the ground electronic state, the minimum of the charge-transfer potential could be reached so that the crossings with the repulsive states could be avoided. From there, the reaction could then proceed by changing the intermolecular coordinates while evolving on this particular electronic state. The emission from this state, for example, could be then used as an indication of the control of the excitation process.

The fs-CARS process, as can readily be seen by comparing Figures 2.1 and 3.8, offers the means for this kind of control scheme, as it consists of the process of generation and interrogation of the ground state vibrational wavepacket. The change from the study of the wavepacket to the control of the reaction would consist of simply changing the probe wavelength to correspond to the appropriate excitation energy. In principle, the charge-transfer reaction could be controlled also with a simpler pulse sequence via a wavepacket on the B state of iodine similarly to the I_2–Xe harpooning reaction studies of Potter *et al.*,[31] but the new approach considered here is the possibility to use the ground electronic state vibrational wavepackets for

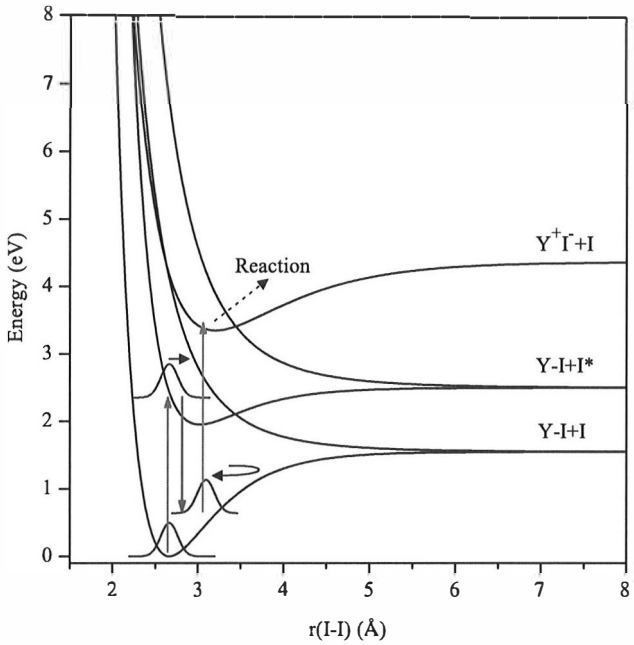

Figure 3.8: A simplified presentation of the proposed control scheme for the iodine complexes, with Y being the species complexed with the iodine molecule. The arrows represent the femtosecond laser pulses that could be used to control the charge-transfer reaction by exploiting the evolution of a vibrational wavepacket on the ground electronic state of the system. The presentation shows only the I-I coordinate of the system, but in the actual reaction also other coordinates, especially the intermolecular coordinate, will change.

this purpose. The use of the ground electronic state as the starting point may be advantageous in general, because it does not have any crossings with repulsive states, so the wavepacket will be long-lived and predissociation is not a problem.

The realization of this kind of reaction control in a bimolecular complex with predesigned pulses requires detailed information on the properties of the ground and excited states of the complex, as well as on the evolution of the wavepacket and the dephasing times on the ground electronic state. To initiate the process, the probability for the creation of the wavepacket

has to be high enough, and the wavepacket should not dephase before reaching the desired conformation. Also, the excited state potentials have to be well known to be able to design the final exciting pulse, and to explain and understand the outcomes of the control experiments. The aim of this work was in part to clarify these questions for I_2–Xe and I_2–Bz complexes, and to evaluate the value of these two systems as possible prototypes for realizing the proposed control scheme.

3.4.2 I_2–Xe and I_2–Bz as model systems for reaction control

The work presented in this thesis has given plenty of new information on both of the I_2–Xe and I_2–Bz complexes isolated in solid krypton. The ground-state structure of both complexes is verified, and the spectroscopic parameters for the iodine vibration in both complexes are determined with high accuracy, describing the ground electronic state potential. The dephasing rates of the ground-state vibrations are also determined for both complexes, and very high vibrational wavepackets were succesfully excited in the I_2–Xe complex.

The primary condition for realizing the reaction control scheme based on the fs-CARS process is to be able to excite the wavepacket with high enough vibrational eigenstates on the ground electronic state. The term "high enough" is determined by the position on the potential surface that the wavepacket needs to reach in order to realize the final excitation in a desired way. For the I_2–Bz complex, the potential minimum of the charge-transfer state is located at the I–I bond length of approximately 3.2 Å.[113,114,139] To reach this bond length, approximately states with $v \geq 20$ on the ground electronic state of I_2–Bz complex should be excited, although even a smaller bond length might suffice, depending on the exact position of the crossings of the repulsive and bound states. However, only states up to $v = 8$ were succesfully excited in our resonance Raman scattering experiments, and in the fs-CARS experiments no signal from the complex was detected. The fs-CARS experiments might be more succesful with different pulse wavelengths as discussed in Section 3.3, but definitely a more thorough study of the fs-CARS process in the I_2–Bz complex is needed. Also, the fast decaying intensity of the Raman lines of the complex, suggesting a faster dephasing on the excited electronic state, might indicate difficulties in exciting high vibrational wavepackets using a Raman process, as for the creation of the wavepacket with higher vibrational eigenstates on the ground electronic state, the electronic wavepacket has to evolve longer on the excited state to reach the optimum conformation.[59,60]

For the I_2–Xe complex, the excitation of wavepackets with high vibrational states using fs-CARS process was succesful, and the strong signal obtained for the $v = 19$–22 superposition suggests, that excitation of even higher states is readily possible. The vibrational level structure is now well known for the I–I vibration in the complex, enabling designing the pump-dump pulse sequence accurately to reach the desired eigenstates. Thus, the fs-CARS process can be used to manipulate and interrogate the complex vibrations in a wide distribution of ground electronic state vibrational levels, making the control process, from this point of view, realizable. It should be noted, that the fs-CARS signal of the complex was only visible in the polarization beats, so the rather small concentration of the I_2–Xe complex in the sample may make the experiment demanding from the detection point of view. However, the amount of complexes may be increased in the sample by adding more xenon to the sample, if care is taken in the sample preparation that larger clusters are not created.

The dephasing of the vibrational wavepacket on the ground electronic state needs also to be taken into account when considering the applicability of these complexes as model systems for the reaction control experiments. One reason for realizing the control via vibrational wavepackets on the ground electronic state instead of excited electronic states is the long lifetime of the coherence, which may be helpful if the evolution part of the process needs to be long in order to reach the right position and shape for the wavepacket, or to eliminate competing processes with shorter dephasing times. From this point of view, both the I_2–Bz and I_2–Xe complexes are good candidates for the control experiments, as the measured vibrational dephasing times allow for tens to hundreds of round-trips of the vibrational wavepacket on the ground electronic state potential before dephasing.

When aiming for coherent control using predesigned laser pulse sequence, also the electronic state potentials relevant to the control sequence should be well known to be able to design the pulses and explain the results. In this work, mainly the ground electronic state potentials were studied for both complexes, with only some suggestions on the excited B state dynamics from the intensities in the resonance Raman spectra. For the ground electronic state, the structure of the complexes were determined and confirmed experimentally. The vibrational level structure was also determined, from which the properties of the ground state potential curve can be deduced. The I_2–Xe complex was found to be well described with a Morse potential up to $v = 22$, while the experimental information obtained on the I_2–Bz complex was limited to $v_{max} = 8$. The excited state potentials, on the other hand, are not so well known for either of the complexes, especially in solid krypton. As can be seen from the UV-vis measurements for the I_2–Bz complex,

the electronic state potentials are, however, affected both by the complexation and also by the isolation in the matrix. Thus, to accurately plan and explain the control experiments, more detailed information on the excited state potentials would be desirable, experimentally or computationally.

In conclusion, the I_2–Xe or I_2–Bz complexes isolated in solid krypton can both be considered further as model systems for the coherent control of bimolecular reaction using the fs-CARS scheme with predesigned femtosecond pulse sequence. For the time being, the I_2–Xe complex seems to be the more attractive case, because the excitation of high vibrational wavepackets on the ground electronic state has already been successful. However, when considering the other properties of the complexes, both seem to have the qualities that support their use in such experiments, such as long vibrational dephasing times and well known vibrational level structure on the ground electronic state.

At the writing of this thesis, the coherent control of a bimolecular reaction using predesigned fs-CARS pulse sequence has not yet been accomplished. However, the work presented here might bring it one step closer, by presenting several important details and outlining a possible recipe for its realization. Should the control scheme work in the solid model system with isolated 1:1 complexes, it might be applicable also to solid, liquid, and even gas phase, bringing the coherent control of bimolecular reactions ever closer to real-life applications. However, only future can tell how far this work will carry us.

4 Conclusions

In the work presented in this thesis, iodine molecule and its 1:1 complexes with xenon atom and benzene molecule isolated in low-temperature solid krypton environment were studied experimentally using several spectroscopic methods including UV-vis and FTIR absorption, resonance Raman and femtosecond coherent anti-Stokes Raman scattering (fs-CARS) measurements. The results for each system include the vibrational parameters for iodine molecule on the ground electronic state of the system, the dephasing rates for the ground state vibrations, the dephasing mechanism, and the structures for both of the complexes.

In the case of I_2–Xe and I_2–Bz samples, polarization interference between the different molecular species in the sample was detected in the fs-CARS signal. This interference was shown to be a useful spectroscopic tool, with which the properties of a weak signal species could be determined. The use of polarization beating as an "amplifier" was demonstrated for both a low concentration species (I_2–Xe complex) and electronically nonresonant species (benzene molecule). The polarization beats were succesfully used to find out the properties of these systems.

Additionally, a general recipe for executing coherent control of a bimolecular charge-transfer reaction using a fs-CARS scheme was outlined. The experimental results obtained for the I_2–Xe and I_2–Bz complexes in this work were evaluated from the reaction control point of view. More detailed information is still needed on the excited potential energy surfaces of the system in order to execute the scheme with a predesigned pulse sequence for both complexes, and for the I_2–Bz complex, further studies on the fs-CARS process are necessary. However, in the light of the results presented here, no general constraints against realizing the scheme were found, and both complexes can be considered as good model systems for the control experiment.

Bibliography

1. L. R. Khundkar and A. H. Zewail, *Annu. Rev. Phys. Chem.*, **1990**, *41*, 15–60.
2. A. H. Zewail, *Pure Appl. Chem.*, **2000**, *72*, 2219–2231.
3. A. H. Zewail, *Science*, **1988**, *242*, 1645–1653.
4. M. Dantus, *Annu. Rev. Phys. Chem.*, **2001**, *52*, 639–679.
5. M. Nisoli and G. Sansone, *Prog. Quantum Electron.*, **2009**, *33*, 17–59.
6. A. H. Zewail, *Phys. Today*, **1980**, *33*, 27 33.
7. P. Brumer and M. Shapiro, *Annu. Rev. Phys. Chem.*, **1992**, *43*, 257–282.
8. R. J. Gordon and S. A. Rice, *Annu. Rev. Phys. Chem.*, **1997**, *48*, 601–641.
9. S. A. Rice, *Nature*, **2001**, *409*, 422–426.
10. T. Brixner and G. Gerber, *ChemPhysChem*, **2003**, *4*, 418–438.
11. M. Dantus and V. V. Lozovoy, *Chem. Rev.*, **2004**, *104*, 1813–1859.
12. K. Ohmori, *Annu. Rev. Phys. Chem.*, **2009**, *60*, 487–511.
13. Y. Silberberg, *Annu. Rev. Phys. Chem.*, **2009**, *60*, 277 292.
14. P. Nuernberger, G. Vogt, T. Brixner, and G. Gerber, *Phys. Chem. Chem. Phys.*, **2007**, *9*, 2470–2497.
15. W. S. Warren, H. Rabitz, and M. Dahleh, *Science*, **1993**, *259*, 1581–1589.
16. D. J. Tannor, *Introduction to Quantum Mechanics: A Time-Dependent Perspective*, University Science Books, Sausalito, **2006**.

17. D. J. Tannor and S. A. Rice, *J. Chem. Phys.*, **1985**, *83*, 5013–5018.

18. D. J. Tannor, R. Kosloff, and S. A. Rice, *J. Chem. Phys.*, **1986**, *85*, 5805–5820.

19. M. Shapiro and P. Brumer, *J. Chem. Phys.*, **1986**, *84*, 4103–4104.

20. P. Brumer and M. Shapiro, *Acc. Chem. Res.*, **1989**, *22*, 407–413.

21. R. Kosloff, S. A. Rice, P. Gaspard, S. Tersigni, and D. J. Tannor, *Chem. Phys.*, **1989**, *139*, 201–220.

22. I. Pastirk, E. J. Brown, Q. Zhang, and M. Dantus, *J. Chem. Phys.*, **1998**, *108*, 4375–4378.

23. S. Shi and H. Rabitz, *J. Chem. Phys.*, **1990**, *92*, 364–376.

24. A. Assion, T. Baumert, J. Helbing, V. Seyfried, and G. Gerber, *Chem. Phys. Lett.*, **1996**, *259*, 488–494.

25. V. V. Lozovoy, S. A. Antipin, F. E. Gostev, A. A. Titov, D. G. Tovbin, O. M. Sarkisov, A. S. Vetchinkin, and S. Y. Umanskii, *Chem. Phys. Lett.*, **1998**, *284*, 221–229.

26. V. V. Yakovlev, C. J. Bardeen, J. Che, J. Cao, and K. R. Wilson, *J. Chem. Phys.*, **1988**, *108*, 2309–2313.

27. R. S. Judson and H. Rabitz, *Phys. Rev. Lett.*, **1992**, *68*, 1500–1503.

28. C. J. Bardeen, J. Che, K. R. Wilson, V. V. Yakolev, V. A. Apkarian, C. C. Martens, R. Zadoyan, B. Kohler, and M. Messina, *J. Chem. Phys.*, **1997**, *106*, 8486–8503.

29. A. Assion, T. Baumert, M. Bergt, T. Brixner, B. Kiefer, V. Seyfried, M. Strehle, and G. Gerber, *Science*, **1998**, *282*, 919–922.

30. C. J. Bardeen, V. V. Yakolev, K. R. Wilson, S. D. Carpenter, P. M. Weber, and W. S. Warren, *Chem. Phys. Lett.*, **1997**, *280*, 151–158.

31. E. D. Potter, J. L. Herek, S. Pedersen, Q. Liu, and A. H. Zewail, *Nature*, **1992**, *355*, 66–68.

32. V. A. Apkarian, *J. Chem. Phys.*, **1997**, *106*, 5298–5299.

33. G. Herzberg, *Spectra of Diatomic Molecules*, Van Nostrand Reinhold, New York, **1950**.

34. W. A. de Jong, L. Visscher, and W. C. Nieuwpoort, *J. Chem. Phys.*, **1997**, *107*, 9046–9058.

35. R. M. Bowman, M. Dantus, and A. H. Zewail, *Chem. Phys. Lett.*, **1989**, *161*, 297–302.

36. M. Gruebele, G. Roberts, M. Dantus, R. M. Bowman, and A. H. Zewail, *Chem. Phys. Lett.*, **1990**, *166*, 459–469.

37. M. Dantus, R. M. Bowman, and A. H. Zewail, *Nature*, **1990**, *343*, 737–739.

38. V. Senekerimyan, I. Goldschleger, and V. A. Apkarian, *J. Chem. Phys.*, **2007**, *127*, 214511.

39. R. Zadoyan, M. Sterling, M. Ovchinnikov, and V. A. Apkarian, *J. Chem. Phys.*, **1997**, *107*, 8446–8460.

40. M. Bargheer, M. Gühr, P. Dietrich, and N. Schwentner, *Phys. Chem. Chem. Phys.*, **2002**, *4*, 75–81.

41. M. Gühr, M. Bargheer, P. Dietrich, and N. Schwentner, *J. Phys. Chem. A*, **2002**, *106*, 12002–12011.

42. Z. Bihary, M. Karavitis, and V. A. Apkarian, *J. Chem. Phys.*, **2004**, *120*, 8144–8156.

43. D. Segale, M. Karavitis, E. Fredj, and V. A. Apkarian, *J. Chem. Phys.*, **2005**, *122*, 111104.

44. A. Scaria, V. Namboodiri, J. Konradi, and A. Materny, *J. Chem. Phys.*, **2007**, *127*, 144305.

45. ●. Liu, J.-K. Wang, and A. H. Zewail, *Nature*, **1993**, *364*, 427–430.

46. R. Zadoyan, Z. Li, P. Ashjian, C. C. Martens, and V. A. Apkarian, *Chem. Phys. Lett.*, **1994**, *218*, 504–514.

47. C. Wan, M. Gupta, J. S. Baskin, Z. H. Kim, and A. H. Zewail, *J. Chem. Phys.*, **1997**, *106*, 4353–4356.

48. Z. Bihary, R. Zadoyan, M. Karavitis, and V. A. Apkarian, *J. Chem. Phys.*, **2004**, *120*, 7576–7589.

49. J. Almy, K. Kizer, R. Zadoyan, and V. A. Apkarian, *J. Phys. Chem. A*, **2000**, *104*, 3508–3520.

50. W. Holzer, W. F. Murphy, and H. J. Bernstein, *J. Chem. Phys.*, **1970**, *52*, 399–407.

51. J. M. Grzybowski and L. Andrews, *J. Raman Spectrosc.*, **1975**, *4*, 99–113.

52. V. V. Lozovoy, I. Pastirk, E. J. Brown, B. I. Grimberg, and M. Dantus, *Int. Rev. Phys. Chem.*, **2000**, *19*, 531–552.

53. M. Schmitt, G. Knopp, A. Materny, and W. Kiefer, *Chem. Phys. Lett.*, **1997**, *280*, 339–347.

54. E. J. Brown, I. Pastirk, B. I. Grimberg, and V. V. Lozovoy, *J. Chem. Phys.*, **1999**, *111*, 3779–3782.

55. I. Pastirk, V. V. Lozovoy, B. I. Grimberg, E. J. Brown, and M. Dantus, *J. Phys. Chem. A*, **1999**, *103*, 10226–10236.

56. V. V. Lozovoy, B. I. Grimberg, E. J. Brown, I. Pastirk, and M. Dantus, *J. Raman Spectrosc.*, **2000**, *31*, 41–49.

57. T. Siebert, M. Schmitt, A. Vierheilig, G. Flachenecker, V. Engel, A. Materny, and W. Kiefer, *J. Raman Spectrosc.*, **2000**, *31*, 25–31.

58. A. Materny, T. Chen, M. Schmitt, T. Siebert, A. Vierheilig, V. Engel, and W. Kiefer, *Appl. Phys. B*, **2000**, *71*, 299–317.

59. G. Knopp, I. Pinkas, and Y. Prior, *J. Raman Spectrosc.*, **2000**, *31*, 51–58.

60. I. Pinkas, G. Knopp, and Y. Prior, *J. Chem. Phys.*, **2001**, *115*, 236–244.

61. M. Schmitt, G. Knopp, A. Materny, and W. Kiefer, *Chem. Phys. Lett.*, **1997**, *270*, 9–15.

62. S. Meyer, M. Schmitt, A. Materny, W. Kiefer, and V. Engel, *Chem. Phys. Lett.*, **1997**, *281*, 332–336.

63. M. Schmitt, G. Knopp, A. Materny, and W. Kiefer, *J. Phys. Chem. A*, **1998**, *102*, 1059–1065.

64. R. Zadoyan and V. A. Apkarian, *Chem. Phys. Lett.*, **2000**, *326*, 1–10.

65. S. Meyer, M. Schmitt, A. Materny, W. Kiefer, and V. Engel, *Chem. Phys. Lett.*, **1998**, *287*, 753–754.

66. S. Meyer and V. Engel, *J. Raman Spectrosc.*, **2000**, *31*, 33–39.

67. R. Lausten, O. Smirnova, B. J. Sussman, S. Gräfe, A. S. Mouritzen, and A. Stolow, *J. Chem. Phys.*, **2008**, *128*, 244310.

68. M. Karavitis, R. Zadoyan, and V. A. Apkarian, *J. Chem. Phys.*, **2001**, *114*, 4131–4140.

69. M. Karavitis, D. Segale, Z. Bihary, M. Pettersson, and V. A. Apkarian, *Low Temp. Phys.*, **2003**, *29*, 814–823.

70. M. Karavitis, T. Kumada, I. U. Goldschleger, and V. A. Apkarian, *Phys. Chem. Chem. Phys.*, **2005**, *7*, 791–796.

71. M. Karavitis and V. A. Apkarian, *J. Chem. Phys.*, **2004**, *120*, 292–299.

72. Z. Bihary, M. Karavitis, R. B. Gerber, and V. A. Apkarian, *J. Chem. Phys.*, **2001**, *115*, 8006–8013.

73. E. T. Sleva, M. Glasbeek, and A. H. Zewail, *J. Phys. Chem.*, **1986**, *90*, 1232–1234.

74. N. F. Scherer, A. J. Ruggiero, M. Du, and G. R. Fleming, *J. Chem. Phys.*, **1990**, *93*, 856–857.

75. N. F. Scherer, R. J. Carlson, A. Matro, M. Du, A. J. Ruggiero, V. Romero-Rochin, J. A. Cina, G. R. Fleming, and S. A. Rice, *J. Chem. Phys.*, **1991**, *96*, 1487–1511.

76. N. F. Scherer, L. D. Ziegler, and G. R. Fleming, *J. Chem. Phys.*, **1992**, *96*, 5544–5547.

77. N. F. Scherer, D. M. Jonas, and G. R. Fleming, *J. Chem. Phys.*, **1993**, *99*, 153–168.

78. B. Kohler, V. V. Yakolev, J. Che, J. L. Krause, M. Messina, K. R. Wilson, N. Schwentner, R. M. Whitnell, and Y. Yan, *Phys. Rev. Lett.*, **1995**, *74*, 3360–3363.

79. B. Kohler, J. L. Krause, F. Raksi, K. R. Wilson, V. V. Yakolev, R. M. Whitnell, and Y. Yan, *Acc. Chem. Res.*, **1995**, *28*, 133–140.

80. M. Bargheer, P. Dietrich, K. Donovang, and N. Schwentner, *J. Chem. Phys.*, **1999**, *111*, 8556–8564.

81. R. Zadoyan, N. Schwentner, and V. A. Apkarian, *Chem. Phys.*, **1998**, *233*, 353–363.

82. C. P. Lin, J. Bates, J. T. Mayer, and W. S. Warren, *J. Chem. Phys.*, **1987**, *86*, 3750–3751.

83. B. I. Grimberg, V. V. Lozovoy, M. Dantus, and S. Mukamel, *J. Phys. Chem. A*, **2002**, *106*, 697–718.

84. V. V. Lozovoy, O. M. Sarkisov, A. S. Vetchinkin, and S. Y. Umanskii, *Chem. Phys.*, **1999**, *243*, 97–114.

85. I. Pastirk, V. V. Lozovoy, and M. Dantus, *Chem. Phys. Lett.*, **2001**, *333*, 76–82.

86. V. V. Lozovoy, B. I. Grimberg, I. Pastirk, and M. Dantus, *Chem. Phys.*, **2001**, *267*, 99–114.

87. J. Faeder, I. Pinkas, G. Knopp, Y. Prior, and D. J. Tannor, *J. Chem. Phys.*, **2001**, *115*, 8440–8454.

88. J. J. Larsen, I. Wendt-Larsen, and H. Stapelfeldt, *Phys. Rev. Lett.*, **1999**, *83*, 1123–1126.

89. V. V. Lozovoy and M. Dantus, *Chem. Phys. Lett.*, **2002**, *351*, 213–221.

90. R. Zadoyan, D. Kohen, D. A. Lidar, and V. A. Apkarian, *Chem. Phys.*, **2001**, *266*, 323–351.

91. Z. Bihary, D. R. Glenn, D. A. Lidar, and V. A. Apkarian, *Chem. Phys. Lett.*, **2002**, *360*, 459–465.

92. D. R. Glenn, D. A. Lidar, and V. A. Apkarian, *Mol. Phys.*, **2006**, *104*, 1249–1266.

93. B. V. O'Grady and R. J. Donovan, *Chem. Phys. Lett.*, **1985**, *122*, 503–506.

94. R. J. Donovan, P. Greenhill, M. A. MacDonald, A. J. Yencha, W. S. Hartree, K. Johnson, C. Jouvet, A. Kvaran, and J. P. Simons, *Faraday Discuss. Chem. Soc.*, **1987**, *84*, 221–238.

95. R. J. Donovan, A. J. Holmes, P. R. R. Langridge-Smith, and T. Ridely, *J. Chem. Soc. Faraday Trans. 2*, **1988**, *84*, 541–548.

96. J. Qin and D. W. Setser, *Chem. Phys. Lett.*, **1991**, *184*, 121–127.

97. F. Okada, L. Wiedeman, and V. A. Apkarian, *J. Phys. Chem.*, **1989**, *93*, 1267–1272.

98. R. Zadoyan and V. A. Apkarian, *Chem. Phys. Lett.*, **1993**, *206*, 475–482.

99. H. A. Benesi and J. H. Hildebrand, *J. Am. Chem. Soc.*, **1948**, *70*, 2832–2833.

100. H. A. Benesi and J. H. Hildebrand, *J. Am. Chem. Soc.*, **1949**, *71*, 2703–2707.

101. K.-F. Weng, Y. Shi, X. Zheng, and D. L. Phillips, *J. Phys. Chem. A*, **2006**, *110*, 851–860.

102. D. Zhong and A. H. Zewail, *J. Phys. Chem A*, **1998**, *102*, 4031–4058.

103. A. M. Mebel, H. L. Lin, and S. H. Lin, *Int. J. Quant. Chem.*, **1999**, *72*, 307–318.

104. F. C. Grozema, R. W. J. Zijlstra, M. Swart, and P. T. van Duijnen, *Int. J. Quant. Chem.*, **1999**, *75*, 709–723.

105. M. Besnard, N. Del Campo, R. M. Cavagnat, and J. Lascombe, *Chem. Phys. Lett.*, **1989**, *162*, 132–136.

106. L. Fredin and B. Nelander, *J. Am. Chem. Soc.*, **1974**, *96*, 1672–1673.

107. H. Rosen, Y. R. Shen, and F. Stenman, *Mol. Phys.*, **1971**, *22*, 33–47.

108. Y. R. Shen, H. Rosen, and F. Stenman, *Chem. Phys. Lett.*, **1968**, *1*, 671–674.

109. J. Yarwood and W. B. Person, *J. Am. Chem. Soc.*, **1968**, *90*, 594–600.

110. P. Klaboe, *J. Am. Chem. Soc.*, **1967**, *89*, 3667–3676.

111. H. Stammreich, R. Forneris, and Y. Tavares, *Spectrochim. Acta*, **1961**, *17*, 1173–1184.

112. J. Lascombe and M. Besnard, *Mol. Phys.*, **1986**, *58*, 573–592.

113. P. Y. Cheng, D. Zhong, and A. H. Zewail, *J. Chem. Phys.*, **1996**, *105*, 6216–6248.

114. G. DeBoer, J. W. Burnett, A. Fujimoto, and M. A. Young, *J. Phys. Chem.*, **1996**, *100*, 14882–14891.

115. G. DeBoer, J. W. Burnett, and M. A. Young, *Chem. Phys. Lett.*, **1996**, *259*, 368–374.

116. P. Y. Cheng, D. Zhong, and A. H. Zewail, *J. Chem. Phys.*, **1995**, *103*, 5153–5156.

117. E. Whittle, D. A. Dows, and G. C. Pimentel, *J. Chem. Phys.*, **1954**, *44*, 1943.

118. I. Norman and G. Porter, *Nature*, **1954**, *174*, 508–509.

119. H. E. Hallam, Ed., *Vibrational Spectroscopy of Trapped Species*, John Wiley & Sons, London, **1973**.

120. I. R. Dunkin, *Matrix-Isolation Techniques - A Practical Approach*, Oxford University Press, New York, **1998**.

121. S. Mukamel, *Principles of Nonlinear Optical Spectroscopy*, Oxford University Press, New York, **1999**.

122. C. Rulliére, Ed., *Femtosecond Laser Pulses - Principles and Experiments*, Springer-Verlag, Berlin Heidelberg, **1998**.

123. D. J. Tannor, S. A. Rice, and P. M. Weber, *J. Chem. Phys.*, **1985**, *83*, 6158–6164.

124. S. Meyer, M. Schmitt, A. Materny, W. Kiefer, and V. Engel, *Chem. Phys. Lett.*, **1999**, *301*, 248–254.

125. J. L. Skinner, *Ann. Rev. Phys. Chem.*, **1988**, *39*, 463–478.

126. A. Laubereau and W. Kaiser, *Rev. Mod. Phys.*, **1978**, *50*, 607 665.

127. J. L. Skinner and D. Hsu, *Chem. Phys.*, **1988**, *128*, 35–45.

128. D. W. Oxtoby, *Annu. Rev. Phys. Chem.*, **1981**, *32*, 77 101.

129. D. J. Diestler and A. H. Zewail, *J. Chem. Phys.*, **1979**, *71*, 3103–3112.

130. R. Leonhardt, W. Holzapfel, W. Zinth, and W. Kaiser, *Chem. Phys. Lett.*, **1987**, *133*, 373–377.

131. O. Rubner, M. Schmitt, G. Knopp, A. Materny, W. Kiefer, and V. Engel, *J. Phys. Chem. A*, **1998**, *102*, 9734–9738.

132. T. Joo, M. A. Dugan, and A. C. Albrecht, *Chem. Phys. Lett.*, **1991**, *177*, 4–10.

133. M. Koch, J. Feldmann, G. von Plessen, E. O. Göbel, P. Thomas, and K. Köhler, *Phys. Rev. Lett.*, **1992**, *69*, 3631–3634.

134. V. G. Lyssenko, J. Erland, I. Balslev, K.-H. Pantke, B. S. Razbirin, and J. M. Hvam, *Phys. Rev. B*, **1993**, *48*, 5720–5723.

135. M. Hayashi, M. Sugawara, and Y. Fujimura, *Phys. Rev. A*, **1991**, *43*, 2416–2429.

136. L. Fredin and B. Nelander, *Mol. Phys.*, **1974**, *27*, 885–898.

137. G. Kerenskaya, I. U. Goldschleger, V. A. Apkarian, E. Fleischer, and K. C. Janda, *J. Phys. Chem. A*, **2007**, *111*, 10969–10976.

138. J. Tellinghuisen, *J. Chem. Phys.*, **1982**, *76*, 4736–4744.

139. E. C. M. Chen and W. E. Wentworth, *J. Phys. Chem.*, **1985**, *89*, 4099–4105.

ORIGINAL PAPERS

I

Time-resolved coherent anti-Stokes Raman-scattering measurements of I_2 in solid Kr: Vibrational dephasing on the ground electronic state at 2.6–32 K.

by

Tiina Kiviniemi, Jukka Aumanen, Pasi Myllyperkiö,
V. Ara Apkarian, and Mika Pettersson, 2005.

Journal of Chemical Physics **2005**, *123*, 064509.

https://doi.org/10.1063/1.1990115

II

Time-resolved coherent anti-Stokes Raman-scattering polarization beat spectroscopy of I_2–Xe complex in solid krypton.

by

Tiina Kiviniemi, Toni Kiljunen, and Mika Pettersson, 2006.

Journal of Chemical Physics **2006**, *125*, 164302.

https://doi.org/10.1063/1.2358987

III

Vibrational Characterization of the 1:1 Iodine–Benzene Complex Isolated in Solid Krypton.

by

Tiina Kiviniemi, Eero Hulkko, Toni Kiljunen, and Mika Pettersson, 2008.

Journal of Physical Chemistry A **2008**, *112*, 5025—5027.

https://doi.org/10.1021/jp801980k

IV

Iodine–Benzene Complex as a Candidate for a Real-Time Control of a Bimolecular Reaction. Spectroscopic Studies of the Properties of the 1:1 Complex Isolated in Solid Krypton.

by

Tiina Kiviniemi, Eero Hulkko, Toni Kiljunen, and Mika Pettersson, 2009.

Journal of Physical Chemistry A **2009**, *113*, 6326–6333.

https://doi.org/10.1021/jp902012u

V

Impulsive excitation of high vibrational states in a I_2–Xe complex on the electronic ground state.

by

Tiina Kiviniemi, Eero Hulkko, and Mika Pettersson, 2010.

Chemical Physics Letters **2010**, *491*, 44–48.

https://doi.org/10.1016/j.cplett.2010.03.075